Published online 29 May 2023

Nucleic Acids Research, 2023, Vol. 51, No. 13 ***6981–6998***
https://doi.org/10.1093/nar/gkad469

NOVA1 prevents overactivation of the unfolded protein response and facilitates chromatin access during human white adipogenesis

Zhigang Yang[1,2,*,†], Ping Dong[1,†], Jiankun Cao[1,†], Na Lin[1,†], Shize Ma[1,2], Rui Cao[1,2], Lei Cai[1], Lei Wang[3], Changchang Cao[3], Yuanchao Xue[3], Jing Pan[1], Xiu Li[1,2], Kang Wang[1], Qiwei Liu[1,2], Chen Li[1,2], Fuxing Gong[1,2], Xin Fu[1,2] and Ran Xiao[1,2,*]

[1]Plastic Surgery Hospital, Chinese Academy of Medical Sciences and Peking Union Medical College, Beijing 100144, China, [2]Key Laboratory of External Tissue and Organ Regeneration, Chinese Academy of Medical Sciences, Beijing 100144, China and [3]Key Laboratory of RNA Biology, Institute of Biophysics, Chinese Academy of Sciences, Beijing 100101, China

Received February 27, 2023; Revised April 25, 2023; Editorial Decision May 09, 2023; Accepted May 15, 2023

ABSTRACT

The molecular mechanism underlying white adipogenesis in humans has not been fully elucidated beyond the transcriptional level. Here, we found that the RNA-binding protein NOVA1 is required for the adipogenic differentiation of human mesenchymal stem cells. By thoroughly exploring the interactions between NOVA1 and its binding RNA, we proved that NOVA1 deficiency resulted in the aberrant splicing of DNAJC10 with an in-frame premature stop codon, reduced DNAJC10 expression at the protein level and hyperactivation of the unfolded protein response (UPR). Moreover, NOVA1 knockdown abrogated the down-regulation of NCOR2 during adipogenesis and up-regulated the 47b+ splicing isoform, which led to decreased chromatin accessibility at the loci of lipid metabolism genes. Interestingly, these effects on human adipogenesis could not be recapitulated in mice. Further analysis of multispecies genomes and transcriptomes indicated that NOVA1-targeted RNA splicing is evolutionarily regulated. Our findings provide evidence for human-specific roles of NOVA1 in coordinating splicing and cell organelle functions during white adipogenesis.

GRAPHICAL ABSTRACT

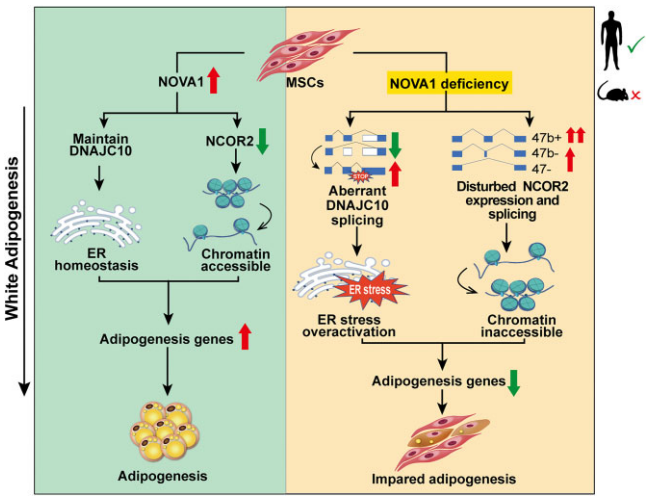

INTRODUCTION

White adipose tissue serves as a critical regulator of systemic energy balance and glucose homeostasis, behind which the adipocyte is regarded as a central player and at the epicenter of a global pandemic of metabolic diseases (1). Adipogenesis, a physiological process whereby fibroblast-like adipose stem or progenitor cells differentiate into specialized, spherical, mature adipocytes, is characterized by increased lipid synthesis and accumulation, and *de novo* formation of lipid droplets. The process is tightly regulated by a complex and highly orchestrated gene expression network. Based on several cell differentiation models and *in vivo* adipose tissue responses to diet or

*To whom correspondence should be addressed. Tel: +86 10 53968226; Fax: +86 10 53968227; Email: xiaoran@psh.pumc.edu.cn
Correspondence may also be addressed to Zhigang Yang. Email: yangzg@psh.pumc.edu.cn
†The authors wish it to be known that, in their opinion, the first four authors should be regarded as Joint First Authors.

pharmaceutical agents that are mostly observed in mice, the transcription factors peroxisome proliferator-activated receptor gamma (PPARγ) and CCAAT-enhancer-binding protein alpha (C/EBPα) are recognized as the master regulators of adipogenesis, while downstream effectors such as FABP4, FASN, CD36 and Adipoq are responsible for the formation of mature adipocytes (2). However, the global viewpoint of adipogenesis at epigenetic and post-transcriptional levels is far less elucidated, especially for human cells.

The vast majority of human genes undergo alternative splicing (AS) to encode multiple proteins with different functions. Biological processes such as cell development and differentiation require proper spatiotemporal expression of specific AS profiles (3). RNA-binding proteins (RBPs) are master regulators of RNA splicing, and they bind to pre-mRNA to control the differential inclusion or exclusion of portions of a nascent transcript into mature mRNA. RBP-mediated AS has been reported to play significant roles in pre-adipocyte commitment and terminal differentiation (4,5). For example, Sam68 deficiency increases the retention of intron 5 of mTOR (mammalian target of rapamycin), which introduces a premature termination codon and undergoes nonsense-mediated decay (NMD), resulting in lower activation levels of downstream effectors and leading to defective adipogenesis; this also leads to a lean phenotype *in vivo* (6).

NOVA is well known as a family of neuron-specific KH-type RBP proteins (including NOVA1 and NOVA2) that bind to YCAY motifs and regulate alternative splicing and polyadenylation. It was first found in paraneoplastic opsoclonus–myoclonus ataxia (POMA) patients with paraneoplastic neurological disorders (7). NOVA1 is crucial for the survival and development of neurons and is involved in the regulation of AS of neurotransmitter receptors such as GABAAγ2 and GlyRα2 (8,9). Nova1 null mice showed apoptotic death of the brainstem and spinal nerve cells, with motor deficits, progressive dyskinesia and death 7–10 days after birth. Like NOVA1, NOVA2 is also essential for the function of multiple neuronal cell types (10). Moreover, NOVA has been reported to play important roles in metabolic-relevant cells in recent years. Villate Olatz *et al*. revealed that silencing of Nova1 altered the splicing profile and insulin secretion of rodent and human pancreatic beta cells (11). Also, mice whose mature adipocytes are NOVA deficient show increased energy expenditure and glucose tolerance on a high-fat diet (12,13). However, the role of NOVA in white adipogenesis, a major contributor to metabolic disorders, remains unknown in both mice and humans.

In this study, we found that several RBPs experience dynamic changes during the adipogenesis of human adipose-derived stromal/stem cells (hASCs) and that NOVA1 but not NOVA2 is required during adipogenesis. NOVA1 knockdown leads to the significant down-regulation of lipid metabolism genes accompanied by hyperactivation of the unfolded protein response (UPR). Integrating CLIP-seq and RNA-seq data, we identified a repertoire of NOVA1–RNA interactions and the regulated RNA splicing or expression in the process of human adipogenesis. NOVA1-regulated AS and expression of NCOR2 lead to decreased chromatin accessibility at the loci of lipid metabolism genes, and aberrant DNAJC10 splicing caused by NOVA1 deficiency triggers endoplasmic reticulum (ER) stress hyperactivation; in combination, these two phenomena impair the adipogenic differentiation potential of hASCs. Interestingly, these effects could not be recapitulated in mice, *in vivo* or *in vitro*. Multispecies genome and transcriptome comparisons showed that NOVA1-targeted RNA splicing is evolutionarily regulated. Overall, our findings provide evidence for human-specific roles for NOVA1 in white adipogenesis, and novel insights into the role of RBPs in coordinating splicing and cell organelle functions during cell differentiation.

MATERIALS AND METHODS

Culture of hASCs, hBMSCs and mASCs

Human adipose tissue and bone marrow aspirates were obtained from donors during plastic surgery procedures. The collection was approved by the Ethical Committee of Plastic Surgery Hospital, CAMS&PUMC, and written informed consent was obtained from all subjects. Inguinal adipose tissue was obtained from wild-type mice and conditional Nova1 knockout mice. For ASC culture, adipose tissue was washed in phosphate-buffered saline (PBS) and digested for 45 min using 0.1% collagenase (Sigma-Aldrich, USA) under constant shaking at 37°C. The mixture was centrifuged for 5 min at 300 *g*, and the stromal vascular fraction (SVF) was washed once with L-glucose Dulbecco's modified Eagle's medium (DMEM; Thermo Fisher, USA) and then filtered through 100 μm mesh filters. The cells were suspended in a growth medium composed of DMEM with 10% (v/v) fetal bovine serum (FBS; Thermo Fisher, USA), plated on cell culture dishes and cultured at 37°C with 5% CO_2. After reaching 90% confluence, the cells were passaged at a 1:3 ratio. Human bone marrow stromal cells (hBMSCs) were obtained from iliac bone marrow and isolated as described previously (14). Passage 2 or 3 cells were used for experiments.

Mouse models

Nova1-flox mice (C57BL/6 background) with exon 3 flanked by loxP sites were generated at the Shanghai Biomodel Organisms Center using the CRISPR/Cas9 stimulated homologous recombination method. Then mice with targeted alleles were bred with Pdgfra-creER (a kind gift from Professor Cheng Tao) mice to generate conditional Nova1 knockout mice. For the induction of Cre-mediated recombination at the fetal development stage, E15.5 pregnant mice received 4 mg of tamoxifen (20 mg/ml in corn oil; Sigma Aldrich, USA) by oral gavage. Mice were housed with a 12 h light–dark cycle in a controlled climate. All animal experiments were conducted following the guidelines and with prior approval of the Animal Care and Use Committee at the Plastic Surgery Hospital, PUMC.

Adipogenic differentiation and Oil Red O staining

After the cells reached 90% confluence, the culture medium was changed to the adipogenic differentiation medium

consisting of DMEM with 10% (v/v) FBS, 1 μM dexamethasone, 200 μM indomethacin, 0.5 mM 3-isobutyl-1-methylxanthine and 10 μM insulin (Sigma Aldrich, USA), or osteogenic and myogenic induction medium (14). The induction medium was changed every 2 days. The lipid droplets were stained with Oil Red O (Sigma Aldrich, USA) following the previously described methods (15).

Quantitative and conventional RT-PCR

Total RNA was extracted with Trizol reagent (Thermo Fisher, USA), and 1 μg of RNA was reverse transcribed into cDNA using M-MLV reverse transcriptase and oligo(dT) or a random primer (Promega, USA). Quantitative real-time polymerase chain reaction (RT-PCR) was performed using a Fast SYBR Green Master Kit and Light Cycler 480 system (Roche, Switzerland) according to the manufacturer's instructions. The expression level of each target gene was normalized to glyceraldehyde phosphate dehydrogenase (GAPDH) and measured using the comparative CT method (ΔΔCT). PCR master mix (Promega, USA) was used for conventional RT-PCR to detect the splicing isoforms of XBP1, NCOR2 and DNAJC10. The primer sequences used are listed in Supplementary Table S1.

Gene knockdown and overexpression

The knockdown of NOVA1, DNAJC10 and NCOR2 in hASCs or hBMSCs was performed by using the lentivirus short hairpin RNA (shRNA) knockdown vector system PLKO.1 (Addgene, USA). Two NOVA1 shRNA sequences were designed as follows, A, 5′-CCGGCAGACCACCGTTAATCCAGATCTCGAG ATCTGGATTAACGGTGGTCTGTTTTTG-3′; B, 5′ - CCGGACCAAGTCCTCTCCATCTGATCTCGAG ATCAGATGGAGAGGACTTGGTTTTTTG-3′. The DNAJC10 shRNA sequence is 5′-CCGGGCACCAG ACATCTGTAGTAATCTCGAGATTACTACAGATGT CTGGTGCTTTTTG-3′. The NCOR2 shRNA sequence is 5′-CCGGATATGACCAGTGGGAAGAGTCCTCG AGGACTCTTCCCACTGGTCATATTTTTTG-3′. The scramble sequence 5′-CCTAAGGTTAAGTCGCCCT CGCTCGAGCGAGGGCGACTTAACCTTAGG-3′ was taken as a control.

For gene overexpression, the full coding sequence (CDS) of NOVA1 or DNAJC10 was inserted into the pCDH-CMV-MCS-EF1-CoGFP vector (System Biosciences, Mountain View, CA, USA), and named pCDH-NOVA1 and pCDH-DNAJC10, respectively. The empty pCDH-CMV-MCS-EF1-CoGFP vector served as a control. For viral packaging, the shRNA and overexpression vectors were transfected into 293T cells together with psPAX2 and pMD2.G (Addgene, USA) with jetPRIME (Polyplus-transfection, USA). The supernatants containing the virus were collected and concentrated before infecting cells in the presence of 5 mg/ml polybrene (Millipore, USA).

Co-transfection of the splicing NCOR2 minigene and NOVA1

NCOR2 exons (46, 47 and 48) along with 300 bp 5′ and 3′ intronic sequences were synthesized and subcloned into pcDNA3.1(+)-Myc-His B vector. Then, the NCOR2 minigene was co-transfected with shNOVA1 or pCDH-NOVA1 into HEK293T cells. Cells were harvested after 48 h and total RNA was extracted and reverse-transcribed to cDNA. RT-PCR was performed with primers specific to minigene transcripts as follows: NCOR2 forward 5′-TAATACGACTCACTATAGG-3′ and reverse 5′-TAGAAGGCACAGTCGAGG-3′; internal reference forward 5′-TAAACGGGCCCTCTAGACTC-3′ and reverse 5′-GCAGCCGAAAAGCCAAGTC-3′.

Cell treatment with an endoplasmic reticulum stressor

hASCs were pre-treated with an ER stressor (either 200 nM thapsigargin or 2.5 μg/ml tunicamycin; Sigma-Aldrich) for 24 h to check UPR activation at the protein level and then induced to differentiate toward adipocytes in differentiation medium containing thapsigargin or tunicamycin for 5 days to analyze the expression of the lipogenesis gene. To detect the effects of NOVA1 overexpression on UPR activation, hASCs were overexpressed with NOVA1 before the treatment with 50 nM thapsigargin and 50 ng/ml tunicamycin for 12 h.

Western blot analysis

Cells were washed with cold PBS and lysed with western blot lysis buffer (Beyotime, China), and the lysates were centrifuged at 13 400 *g* for 5 min at 4°C. Protein concentrations were quantified using a BCA Assay Kit (Beyotime, China). Proteins were separated by 10% sodium dodecylsulfate–polyacrylamide gel electrophoresis (SDS–PAGE) and transferred onto polyvinylidene fluoride (PVDF) membranes (Millipore, USA). The membrane was incubated overnight at 4°C with antibodies against GAPDH (Wanleibio, China), BIP, PERK, IRE1α, phospho IRE1α, EIF2α and phospho EIF2α (all from Cell Signaling Technology, USA). Horseradish peroxidase (HRP)-conjugated goat anti-rabbit secondary antibody (ZSGB-BIO, China) was incubated with the membrane at 37°C for 1 h. Proteins were detected by chemiluminescence using SuperSignal West Pico (Thermo Fisher, USA) and imaged on a ChemiDoc MP imaging system (Bio-Rad, USA).

Estimation of adipose tissue volume by magnetic resonance imaging (MRI)

First, 4-month-old male and female Pdgfra-creER$^{+/-}$;Nova1$^{flox/flox}$ or Pdgfra-creER$^{-/-}$;Nova1$^{flox/flox}$ mice with an induced knockout at embryonic day 14.5 were anesthetized with 1.5% isoflurane in 100% oxygen using a nose cone. Then, a T1-weighted MRI scan of whole mice was performed on a 7.0 T small animal MRI system (7.0 T MRI System, Agilent, USA) with the following parameters: TE (echo time), 10.34 ms; TR (repetition time), 500 ms; slice thickness, 1 mm; matrix, 256 × 256. The measurement of adipose tissue volume and 3D construction were performed using Materialise Mimics software (v21.0, Belgium).

HTA 2.0 transcriptome microarray assay

Total RNA was isolated with Trizol from cells at the indicated time points in the process of adipogenic differentiation of hASCs infected with lentiviral scramble or shNOVA1. The Ambion® WT Expression Kit was applied for biotinylated cDNA synthesis according to the standard Affymetrix protocol. Then cDNA was hybridized for 16 h at 45°C on a Human Transcriptome Array (HTA) 2.0 chip (Affymetrix, USA) in Hybridization Oven 640 (Thermo Fisher, USA). Gene chips were washed and stained in the Affymetrix Fluidics Station 450 and scanned with the Affymetrix® GeneChip Command Console (AGCC) which was installed in the GeneChip® Scanner 3000 (Thermo Fisher, USA). The data were analyzed with the Robust Multichip Analysis (RMA) algorithm using Affymetrix default analysis settings and global scaling as the normalization method. The differentially expressed genes (DEGS) and AS were analyzed by Transcriptome Analysis Console (TAC) software (Thermo Fisher, USA).

RNA-seq and data analyses

After the quality control of total RNA (RIN $\geq$ 7.0 and a 28S:18S ratio $\geq$ 1.5), sequencing libraries were generated and sequenced by Novogene (Tianjin, China). Briefly, a total amount of 1.5 μg of RNA per sample was used for ample preparations. Sequencing libraries were generated using the NEBNext® Ultra™ Directional RNA Library Prep Kit for Illumina® (NEB, USA) following the manufacturer's instructions, and index codes were added to attribute sequences to each sample. The final libraries were qualified by the Agilent 2100 system and subjected to paired-end sequencing with 150 bp reading length on an Illumina NovaSeq 6000 (Illumina, USA).

The raw data were assessed with FastQC and the low-quality data were filtered with NGSQC. About 60 million clean reads were obtained for each sample, the clean reads were aligned to the reference genome using HISAT2 with default parameters and FPKM (fragments per kilobase of transcript per million mapped reads) for each gene was computed with Subread software. The DEGs were analyzed using DESeq2, and the transcripts were quantified by RSEM; the genes or transcripts were defined as differentially expressed when $|\log2FC| > 1$ and the adjusted *P*-value was <0.05 (adjusted the by Benjamini and Hochberg method). AS was analyzed using rMATs. Functional annotation and enrichment analyses were performed using Metascape (16). Venn diagrams were generated using online tools (http://bioinformatics.psb.ugent.be/webtools/Venn/). Hierarchical clustering analyses for the samples were performed with an FPKM matrix of selected DEGs, and the heatmap was subsequently generated by the R package Pheatmap. IGV (Integrative Genomics Viewer) was applied for the visualization of RNA-seq read alignment and distribution.

Cross-linking and immunoprecipitation sequencing (CLIP-seq)

The full CDS of NOVA1 with an N-terminal Flag-tag was inserted into the pCDH-CMV-MCS-EF1-CoGFP vector. hASCs with overexpression of Nova1-flag tag or control were adipogenically induced for 3 days. The cells were UV irradiated at 400 mJ and collected by scraping the cells from 15 cm plates. The CLIP procedure was performed as previously described (17). In brief, the cross-linked cells were lysed and 15 μg of anti-Flag M2 antibody was applied to pull down NOVA1–RNA covalent complexes. Following micrococcal nuclease treatment, 3′-RNA linker ligation and 5′-end ^{32}P labeling, the immunoprecipitant was separated by SDS–PAGE and transferred to a nitrocellulose membrane. After exposure to X-ray film, a thin region of the membrane corresponding to protein–RNA complexes of the appropriate size was cut. The protein was digested with proteinase K (Takara, Japan) before the extraction of the respective RNA by phenol and chloroform. A 5′ RNA linker was then ligated to free RNA and reverse transcribed using superscript reverse transcriptase III (Thermo Fisher) and amplified by PCR. After deep sequencing, the sequenced reads were first trimmed by removing the 5′-adaptor and 3′-adaptor sequences and then mapped to the human reference genome (hg38) with Bowtie2. Piranha was applied for CLIP-seq peak calling with the parameters: -s -o out2.NOVA.rmDup.peak.bed -p 0.001 -b 20 out1.NOVA.rmDup.bed. MEME software was used for binding motif prediction based on the default parameters (18). Meta profiles were generated with the program ngs.plot (19).

Assay for transposase-accessible chromatin (ATAC) sequencing

hASCs from two biological replicates were pre-infected with lentiviruses encoding scramble, shNOVA1, shNOVA1 and shNCOR2, respectively, and adipogenically induced for 3 days. The nuclei of 600 000–1 000 000 freshly detached cells with > 90% cell viability in each group were extracted. ATAC-seq was performed as previously reported (20), and the sequencing libraries were generated and sequenced by Novogene (Tianjin, China). Briefly, the pellet of nuclei was resuspended and incubated in Tn5 transposase reaction mix at 37°C for 30 min. PCR was performed to amplify the library. After the PCR, libraries were purified using AMPure beads (Beckman, USA) and library quality was assessed with Qubit (Thermo Scientific, USA). Following the clustering of index-coded samples performed on a cBot Cluster Generation System using the TruSeq PE Cluster Kit v3-cBot-HS (Illumina, USA), the library preparations were sequenced on an Illumina Hiseq 2500 platform and 150 bp paired-end reads were generated. After removing the adaptor sequences and low-quality reads, the clean data were aligned to the human genome (hg38) using BWA, and high-quality (MAPQ $\geq$ 13) reads were subjected to peak calling using MACS2 with parameter '-q 0.05 –call-summits –nomodel –shift -100 –extsize 200 –keep-dup all'. R package ChIPseeker was used to annotate peaks and draw a heatmap. After merging the peaks of different groups using 'bedtools merge', the mean reads per million (RPM) of each group in the merge peak was calculated; only peaks with a fold change of RPM >2 were considered differential peaks.

Multiple sequence alignment

Multiple sequence alignment was performed using Clustal Omega (https://www.ebi.ac.uk/Tools/msa/clustalo/) with the default setting. Jalview (21) was applied for the visualization of alignment results and phylogenetic tree calculation.

Statistical analysis

Data were analyzed with Prism 5.0 (Graphpad Software, Inc., USA). All values are expressed as the mean ± standard error of the mean (SEM). Unless otherwise indicated, the differences between the groups were assessed using a two-tailed Student's *t*-test. The results were considered statistically significant at $P < 0.05$.

RESULTS

Splicing factor NOVA1 is required for adipocyte differentiation of hMSCs

RBPs, especially splicing factors, are critical mediators in cell type-specific post-transcriptional control of cellular differentiation, exerting their effects by producing multiple protein variants. Using time-series RBP expression profile analysis of GSE176020 datasets (22), we found that several splicing factors dynamically changed during adipogenic differentiation of hASCs (Figure 1A). Quantitative PCR (qPCR) results verified that among the screened factors, *RBM38* and *NOVA1* were impressively and significantly up-regulated in a time-dependent manner (Figure 1B). The deletion of Rbm38 has been reported to result in a significant reduction of adipocyte size and adipose tissue in mice (23). NOVA2 was barely detected in hASCs and remained unchanged during differentiation (Figure 1B; Supplementary Figure S1A). Therefore, we focused on NOVA1 and found that its up-regulation was specific in adipogenesis, but not in osteogenesis or myogenesis (Figure 1C). At the protein level, NOVA1 was gradually up-regulated and reached a peak at 7 days of induction when most hASCs differentiated into adipocytes *in vitro*, along with an increase in adipocyte signatures such as PPARγ, FABP4, C/EBPα and C/EBPβ (Figure 1D). Consistently, the expression level of NOVA1 in adipose tissue filled with mature adipocytes was ∼5-fold higher than that in the SVF mainly containing mesenchymal progenitor/stem cells and pre-adipocytes (Figure 1E).

To explore the function of NOVA1 during adipogenesis, the gene expression profiles of NOVA1 knockdown hASCs followed by 3 days of adipogenic induction were analyzed using transcriptome arrays. Among 1166 differentially expressed transcripts, genes related to lipid synthesis such as *ACSL1*, *FASN*, *LPL*, *PLIN1*, *LPIN1* and *ADIPOQ* were greatly down-regulated (Figure 1F). NOVA1 knockdown by two shRNA sequences (shNOVA1-A and shNOVA1-B) also significantly suppressed the up-regulation of adipocyte marker genes at the mRNA and protein levels during adipogenic induction, with decreased lipid droplet formation (Figure 1G, H; Supplementary Figure S1B), whereas NOVA1 overexpression promoted the adipogenic potential of hASCs (Supplementary Figure S1C–E). Moreover, significant up-regulation of NOVA1 during adipogenic induction was also confirmed in hBMSCs (Supplementary Figure S1F), and the knockdown or overexpression of NOVA1 showed similar inhibiting or promoting effects on the adipogenesis of hBMSCs (Supplementary Figure S1G–J). These results demonstrated that NOVA1 is required for the adipogenesis of hMSCs.

NOVA1 protects hASCs from UPR hyperactivation during adipogenesis

To explore cellular processes and splicing events during adipogenesis in which NOVA1 is involved, RNA-seq was performed after 3 days of adipogenic induction in hASCs with or without NOVA1 knockdown. Integrating RNA-seq and transcriptome array data, we identified 261 up-regulated and 305 down-regulated common genes in the NOVA1 knockdown group (Figure 2A; Supplementary Figure S2A). The down-regulated genes were enriched in the processes of 'metabolism of lipids' such as 'triglyceride metabolism' and 'glycerophospholipid biosynthesis' (Figure 2B), which reinforced the finding of impaired adipogenesis induced by NOVA1 knockdown. On the other hand, the up-regulated genes were mainly engaged in 'unfolded protein response (UPR)' or 'PERK regulated gene expression'. The expression of UPR indicators such as *HSPA5* (*BIP*), *EIF2AK3* (*PERK*), *ERN1* (*IRE1α*), *XBP1* and *DDIT3* was universally increased (Figure 2C). The integration of these DEGs into the Wiki pathways of fatty acid biosynthesis, fatty acid β-oxidation and UPR further suggested the essential roles of NOVA1 in these processes (Supplementary Figure S2B–D).

NOVA1 knockdown-induced expression of *ATF4*, *ATF6*, *PPP1R15A* (*GADD34*) and *DDIT3* (CHOP) was confirmed by qRT-PCR (Figure 2D). XBP1, an important component of the UPR, is catalyzed by IRE1 to generate functional spliced XBP1 (XBP1s) with a 26 nt cleavage (24). NOVA1 knockdown enhanced XBP1s in hASCs both before and after adipogenic induction (Figure 2E). The expression of the ER chaperone BIP, eIF2α kinases PERK, p-eIF2α, p-IRE1α and IRE1α was also significantly promoted at the protein level in NOVA1-knockdown hASCs, especially after adipogenic induction (Figure 2F). These results reveal that NOVA1 knockdown triggered the hyperactivation of UPR in hASCs during adipogenesis.

To further clarify the effect of NOVA1 on the UPR, we overexpressed NOVA1 in hASCs and then stimulated ER stress with thapsigargin or tunicamycin. The expression of BIP, PERK, p-IRE1α, IRE1α and p-eIF2α was significantly decreased (Figure 2G). Next, to detect whether hyperactivation of the UPR affects hASCs adipogenesis, we found a dramatically inhibited adipogenesis with negative Oil Red O staining and decreased expression of *PPARγ*, *C/EBPα*, *FABP4*, *ADIPOQ* and *LPL* in ER stress stimulator-treated hASCs (Figure 2H–J). Therefore, these results demonstrate that increased NOVA1 expression during hASC adipogenesis helps to fine-tune the UPR, which is closely involved in adipogenesis and lipogenesis.

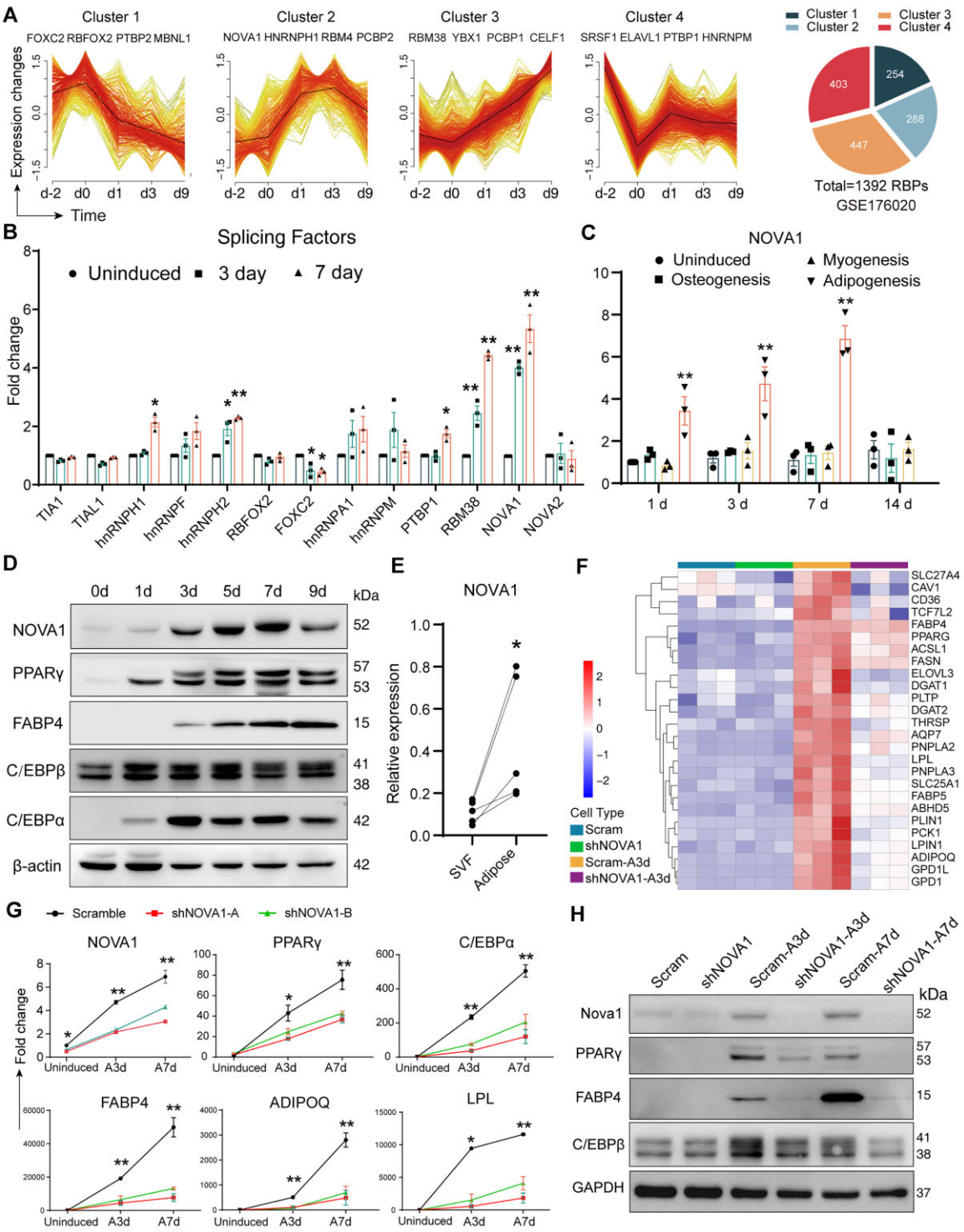

Figure 1. NOVA1 is required for adipogenesis of hASCs. (**A**) Clustering analysis of 1392 RBPs of GSE176020 datasets by Mfuzz. The horizontal axis represents hASCs collected on day –2 (proliferating stage), day 0 (confluent) and on days 1, 3 and 9 of differentiation. The pie chart shows the number of RBPs in each cluster. (**B**) qPCR results showing the dynamic expression of splicing factors at the indicated times following adipogenic induction ($n = 3$). (**C**) Expression of NOVA1 during the differentiation of hASCs toward osteoblasts, myoblasts and adipocytes at the indicated induction times (*, versus uninduced cells, $n = 3$). (**D**) Western blots for NOVA1 and adipogenic markers in hASCs harvested at the indicated adipogenic induction times. Blots are representative of three experiments. (**E**) Expression of NOVA1 in human adipose tissue and the adipose tissue-derived SVF (*, versus SVF, $n = 5$). (**F**) Transcriptome profiles of adipogenic marker genes in control or NOVA1-deficient hASCs. (**G**) Dynamic expression of NOVA1 and adipogenic marker genes in shNOVA1-transduced hASCs at the indicated adipogenic induction times (*, versus the scramble at the same time, $n = 3$). (**H**) Western blots for the effective knockdown of NOVA1 and the down-regulated adipogenic markers in hASCs; the blots are representative of three experiments. Data are shown as means ± SEMs. *P*-values indicate Student's two-tailed *t*-test; *$P < 0.05$, **$P < 0.01$.

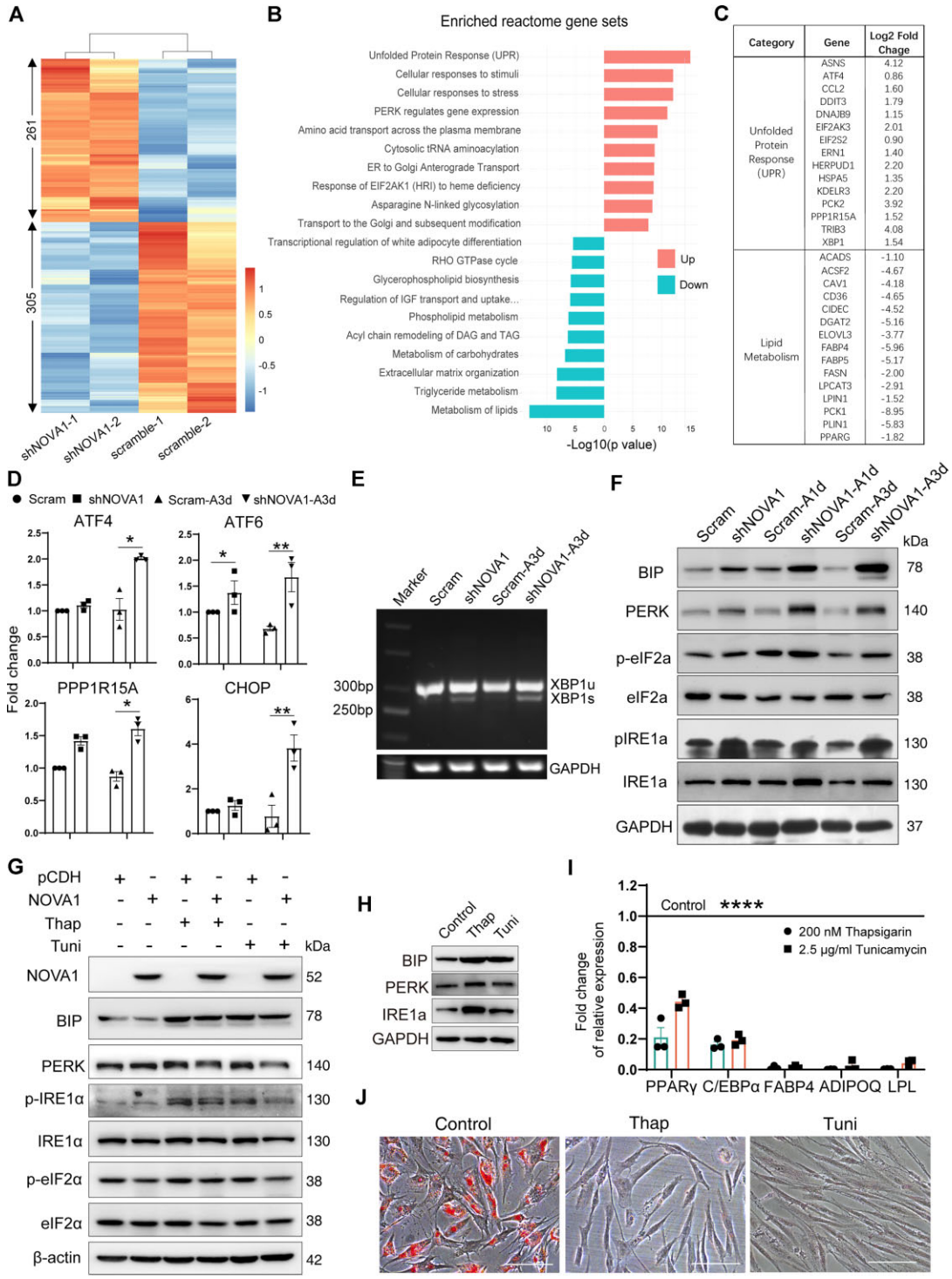

Figure 2. NOVA1 deficiency leads to the hyperactivation of the UPR during adipogenesis of hASCs. (**A**) Transcriptome profiles of common genes by integrating RNA-seq and Affymetrix array of 3 day adipogenically induced hASCs with NOVA1 knockdown. (**B**) The 261 common up-regulated genes are mainly enriched in processes related to the UPR, while the 305 down-regulated genes are enriched in processes related to lipid metabolism. (**C**) Expression changes of genes related to the ER stress pathway and lipid metabolism in NOVA1-knockdown hASCs. (**D**) Expression of UPR-related genes in NOVA1-knockdown hASCs ($n = 3$). (**E**) Enhanced splicing of XBP-1s in NOVA1-knockdown hASCs; the gels are representative of three experiments. (**F**) Western blots showing the dramatically up-regulated UPR indicators in NOVA1-knockdown hASCs, such as BIP, PERK, p-IRE1α and p-eIF2α, especially after adipogenic induction. The blots are representative of four experiments. (**G**) Western blots for the attenuated elevation of BIP, PERK, p-IRE1α, IRE1α and p-eIF2α in NOVA1-overexpressing hASCs stimulated with thapsigargin and tunicamycin. (**H**) Western blots for the UPR indicators activated by thapsigargin and tunicamycin in hASCs. (G) and (H) are representative of three experiments. (**I**) Expression of adipogenic marker genes in hASCs induced for 7 days with thapsigargin or tunicamycin treatment (*, versus control groups, $n = 3$). (**J**) Phase contrast images of Oil Red O staining displaying the abrogated formation of lipid droplets in hASCs treated by thapsigargin or tunicamycin; scale bar = 100 μm. The stainings are representative of four experiments. Data are shown as means ± SEM. *P*-values indicate Student's two-tailed *t*-test; $*P < 0.05$, $**P < 0.01$, $****P < 0.0001$.

CLIP-seq analysis revealed the AS profiles regulated by NOVA1 during adipogenesis

To identify the functional targets of NOVA1 during hASC adipogenesis, we overexpressed NOVA1-flag and studied NOVA1–RNA interactions in the 3 day adipogenically induced hASCs (Supplementary Figure S3A). CLIP-seq identified 61 499 high-confidence non-rRNA peaks that clustered in 10 408 genes. Tags obtained from two biological samples showed a remarkable degree of similarity, with a Pearson correlation coefficient of 0.93, suggesting a robust and highly reproducible NOVA1–RNA interaction in hASCs (Figure 3A; Supplementary Figure S3B). All three motif discovery algorithms demonstrated that CA-rich hexamers were highly enriched in NOVA1-binding clusters, among which the top-scoring motifs were UCAUUC and UCAUCC, with *Z*-scores of 280 and 262.8, respectively (Figure 3B). This is consistent with previously defined NOVA binding characteristics reported in the brains of mice (25). By mapping the sequenced tags to the human genome, we found that 68.48% of the tags were localized in introns (Figure 3C), indicating that most of the tags are derived from pre-mRNAs. A sizable fraction of tags were mapped to non-coding RNAs (3.98%) and intergenic regions (7.59%), implying that NOVA1 may also bind to many non-coding RNAs and/or unannotated transcripts, which will be the subject of future studies. For annotated transcripts, 6.80% of the tags were located in the CDS, 0.37% in the 5′-untranslated region (5′ UTR) and 12.78% in the 3′ UTR, which was supported by the high read density around the 3′ UTR (Figure 3D), indicating that NOVA generally prefers the 3′ UTR in hASCs as well as in neocortex neurons (26).

Furthermore, combining CLIP-seq and RNA-seq, we identified 46 genes with NOVA1-linked AS during hASCs adipogenesis (Figure 3E). Several major modes of AS were found within the 46 genes, including 31 events of selective exon (SE), 4 of retained intron (RI), 6 of mutual exclusive exon cassette (MXE), 8 of alternative 3′ splice (A3SS) and 4 of alternative 5′ splice (A5SS) (Figure 3F). Selected examples were presented (Figure 3G; Supplementary Figure S3C), and differentially expressed transcripts from the above splicing events were compared (Figure 3H). Transcripts down-regulated during adipogenesis (Scram-A3d versus Scram) were dramatically increased in NOVA1-knockdown cells, including transcripts of NCOR2, PDXK and CSF3. In contrast, transcripts of CSAD, LETMD1 and VWCE, which were up-regulated during adipogenesis, were significantly decreased in NOVA1-knockdown cells. Certain transcripts of DNAJC10 and PLEC showed opposite changes. Among these transcripts, DNAJC10 (also named ERDJ5) is an Hsp40-type chaperone and plays an important role in ER-associated degradation (ERAD) of unfolded secretory proteins (27). NCOR2 (also known as SMRT) is a nuclear receptor co-repressor and can act as an adipogenic gatekeeper (28). Therefore, we investigated whether the expression and AS of DNAJC10 or NCOR2 could account for the impaired adipogenesis and UPR hyperactivation caused by NOVA1 deficiency.

NOVA1 deficiency leads to aberrant DNAJC10 splicing and ER stress hyperactivation

The A3SS of DNAJC10 exon 12 generates a longer variant with a partially retained intron 11 containing an in-frame premature stop codon, which triggers NMD, while the inclusion or exclusion of exon 11 gives rise to two protein-coding isoforms (Figure 4A). Visualization of CLIP-seq and RNA-seq data indicated that NOVA1-binding reads clustered around the splicing site, and that the DNAJC10 variant with partial retention of intron 11 within exon 12 obviously increased after NOVA1 knockdown (Figure 4B), which was further confirmed by RT-PCR and qRT-PCR (Figure 4C, D). Together with the down-regulated expression of the two coding transcripts and DNAJC10 protein in NOVA1-silenced hASCs (Figure 4D, E), these results indicate that NOVA1 facilitates the splicing of protein-coding isoforms of DNAJC10 rather than non-coding isoforms.

We further explored whether the decrease in DNAJC10 affected the UPR and adipogenesis. DNAJC10 was knocked down in hASCs before adipogenic induction, and significant elevation of UPR indicators HSPA5 (BIP), PERK and p-IRE1α was observed (Figure 4F). DNAJC10 knockdown also impaired the adipogenic differentiation potential of hASCs, as indicated by decreases in PPARγ expression, the Oil Red O-positive staining area and the expression of adipogenic genes such as *ACSL1*, *CD36*, *FABP4*, *LPL* and *FASN* (Figure 4F–H).

To investigate the role of DNAJC10 in NOVA1-regulated adipogenesis and the UPR, DNAJC10 was overexpressed in hASCs before NOVA1 knockdown. DNAJC10 overexpression partially but significantly rescued the decrease in PPARγ and C/EBPβ expression in NOVA1-knockdown hASCs after 3 days of induction (Figure 5A), and repressed NOVA1 knockdown-induced up-regulation of PERK, p-eIF2a and IRE1a in both undifferentiated and 3 day induced hASCs, although it did not inhibit BIP expression (Figure 5B, C). Moreover, after 7 days of adipogenic induction, the Oil Red O staining and qRT-PCR results showed that DNAJC10 overexpression significantly prevented the decrease in lipid droplets and the expression of *CD36*, *LPL*, *FASN* and *ACSL1* resulting from NOVA1 knockdown (Figure 5D–F). Altogether, these results demonstrate that aberrant DNAJC10 splicing plays a role in NOVA1 knockdown-induced hyperactivation of the UPR and impairment of adipogenesis.

NOVA1 remodels chromatin accessibility by regulating the expression and splicing of NCOR2 during hASC adipogenesis

We carefully checked the transcripts of NCOR2 listed in Figure 3H. Besides the differences in alternative first exons resulting in isoforms with different N-termini, exon 47 is also alternatively spliced and generates isoforms of 47b+, 47b– and 47– (Supplementary Figure S4A, B). The NCOR2 exon 47 alternative splice site maps to the nuclear receptor interaction domain and is known to alter the affinity of the encoded co-repressor protein toward a

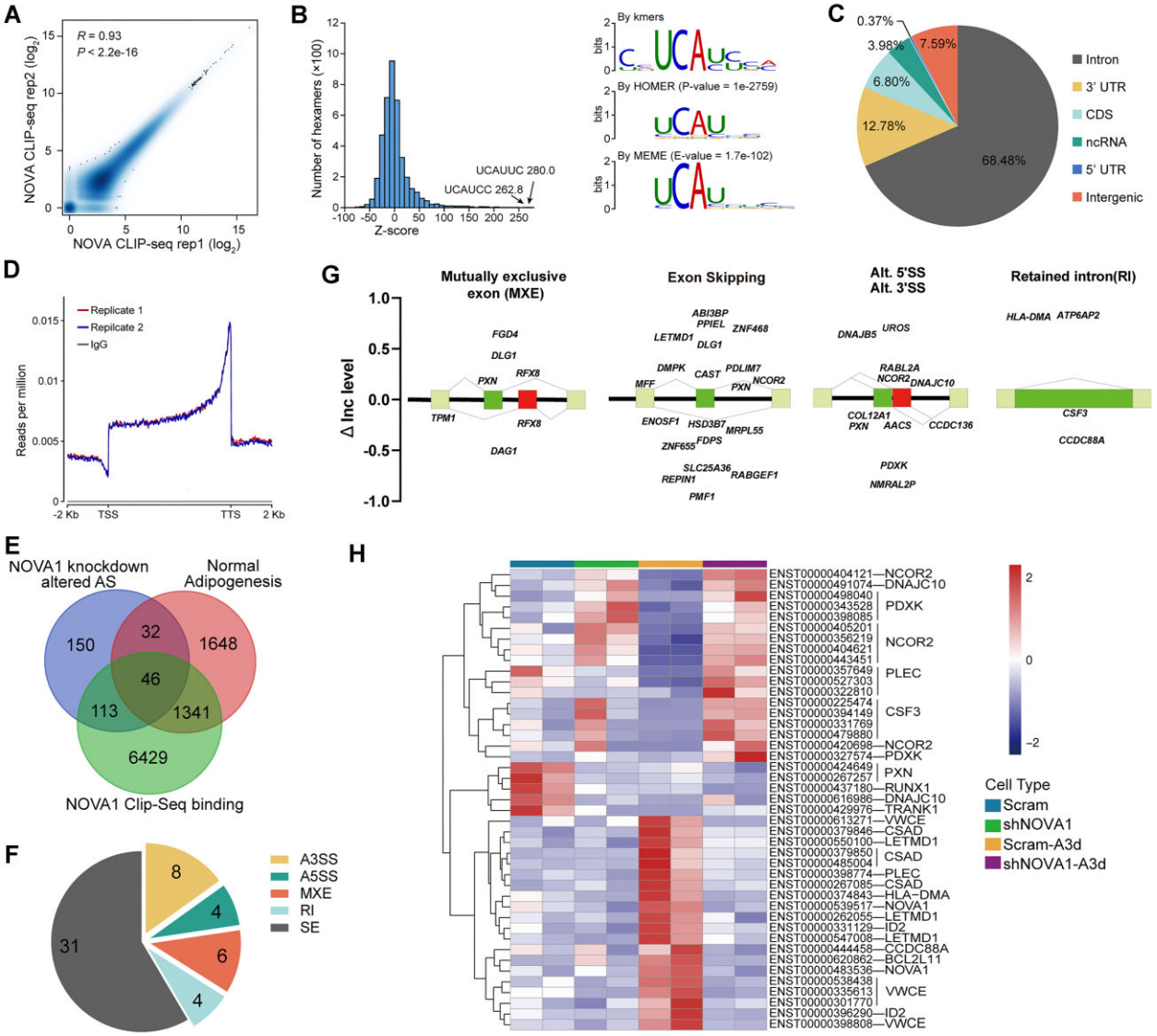

Figure 3. CLIP-seq analysis reveals NOVA1–RNA interactions and regulated splicing during adipogenesis of hASCs. (**A**) Correlation of NOVA1 CLIP-seq replicates. NOVA1 CLIP-seq tags per gene are plotted for two independent biological replicates (Spearman correlation coefficient, $R > 0.93$). (**B**) Over-represented NOVA1-binding motifs identified by CLIP-seq. The histogram of Z-scores indicates the enrichment of hexamers in CLIP-seq clusters compared with randomly chosen regions of similar sizes in the same genes. Z-scores of the top two hexamers are indicated. The right panel shows the NOVA1 binding consensus calculated by three motif discovery algorithms. (**C**) Distribution of NOVA1 CLIP tags in the human genome (hg38). (**D**) Relative distribution profile of CLIP tags along mRNAs, indicating the predominant binding of NOVA1 to the 3′ transcription terminal site. (**E**) Venn diagram of integrating CLIP- and RNA-seq data showing that AS and transcriptome levels of 46 genes bound by NOVA1 were changed. Pie chart (**F**) of different AS modes of the above 46 genes and (**G**) the splicing events of selected genes. (**H**) Differentially expressed transcripts of the 46 genes between scram and NOVA1-knockdown hASCs with or without adipogenic induction.

subset of its nuclear receptor partners (29). Visualization of RNA-seq mapped reads along genomic coordinates showed that the reads corresponding to NCOR2 exons were more frequently detected in NOVA1-deficient cells than in controls (Supplementary Figure S4C), which was consistent with the overall increased expression of NCOR2 splicing variants and was confirmed using qPCR analysis by showing that all three NCOR2 isoforms were up-regulated in NOVA1-knockdown hASCs, especially after adipogenic induction (Figure 6A). Of note, RNA-seq showed an increase in the number of exon 47b splice junctions in NOVA1-knockdown cells (Figure 6B). RT-PCR analysis further showed that NOVA1 knockdown altered the splicing pattern of NCOR2 and increased the ratio of the 47b+ isoform (486 bp) in both undifferentiated and adipogenically induced hASCs (Figure 6C, D). As CLIP-seq indicated that the TCAT motif and the specific binding of NOVA1 were present at the AS site of exon 47, we then constructed a minigene reporter and co-transfected it with NOVA1 shRNA or overexpression plasmid, and found that the expression of NOVA1 greatly affected the splicing of exon 47b (Figure 6B; Supplementary Figure S4D). These results suggest that the up-regulation of NOVA1 during adipogenesis inhibits the

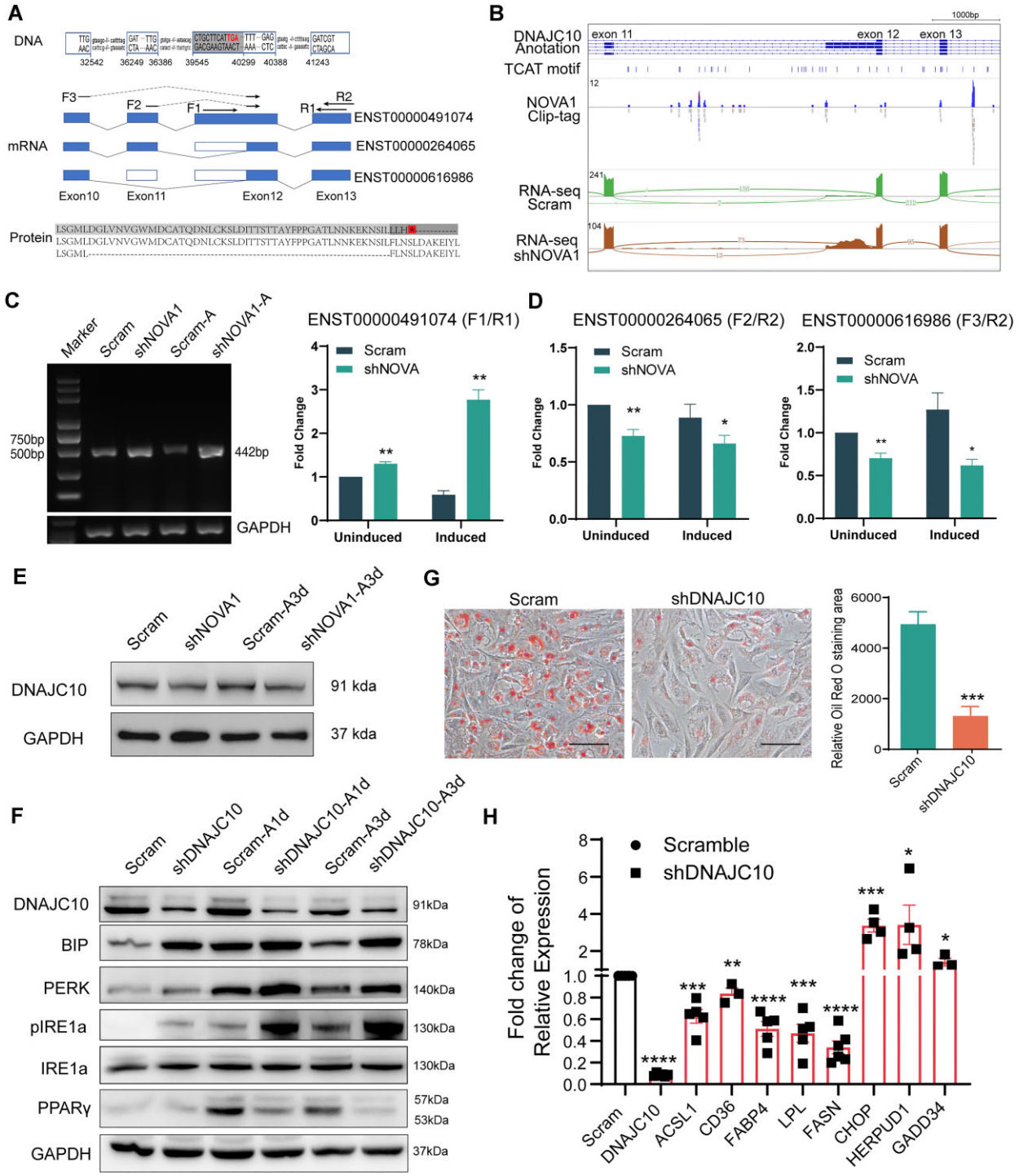

Figure 4. NOVA1 deficiency leads to aberrant DNAJC10 splicing and decreased expression of functional protein. (**A**) Schematic representation of DNAJC10 AS for non-protein-coding and protein-coding transcripts. The A3SS of exon 12 generates the longer isoform with partially retained intron 11, which contains an in-frame premature stop codon (indicated by a red TGA in DNA sequences and by * with a red background in protein sequences); the inclusion or exclusion of exon 11 generates two protein-coding isoforms. The numbers below the DNA sequence indicate the starting and ending position of an exon within the chromosome. The exon junction primers for detecting the expression of specific transcripts are indicated above the corresponding exons of mRNA. (**B**) IGV view of CLIP-seq and RNA-seq data at exons 11–13 of the DNAJC10 locus showing the changed expression level and splicing pattern of DNAJC10, and the binding of NOVA1 upstream of the splicing site. Images are representative of two experiments. (**C** and **D**) Increased expression of the non-protein-coding isoform of DNAJC10 and decreased expression of protein-coding isoforms in NOVA1-knockdown hASCs with or without adipogenic induction (*, versus the scram under the same condition, $n = 3$–8). (**E**) Western blots for the reduced expression of DNAJC10 protein in NOVA1-knockdown hASCs. (**F**) Western blots for the activation of BIP, PERK and p-IRE1α, and inhibition of PPARγ in DNAJC10 knockdown hASCs at the indicated days of differentiation. (**G**) Oil Red O staining of DNAJC10-deficient hASCs ($n = 3$). (E), (F) and (G) are representative of three experiments. (**H**) Real-time PCR showing the efficient knockdown of DNAJC10, the suppressed expression of adipogenic marker genes and stimulation of UPR signals in DNAJC10-deficient hASCs after 7 days of adipogenic induction (*, versus the scram group, $n = 3$–6). Data are shown as means ± SEMs. *P*-values indicate Student's two-tailed *t*-test; $*P < 0.05$, $**P < 0.01$, $***P < 0.001$, $****P < 0.0001$.

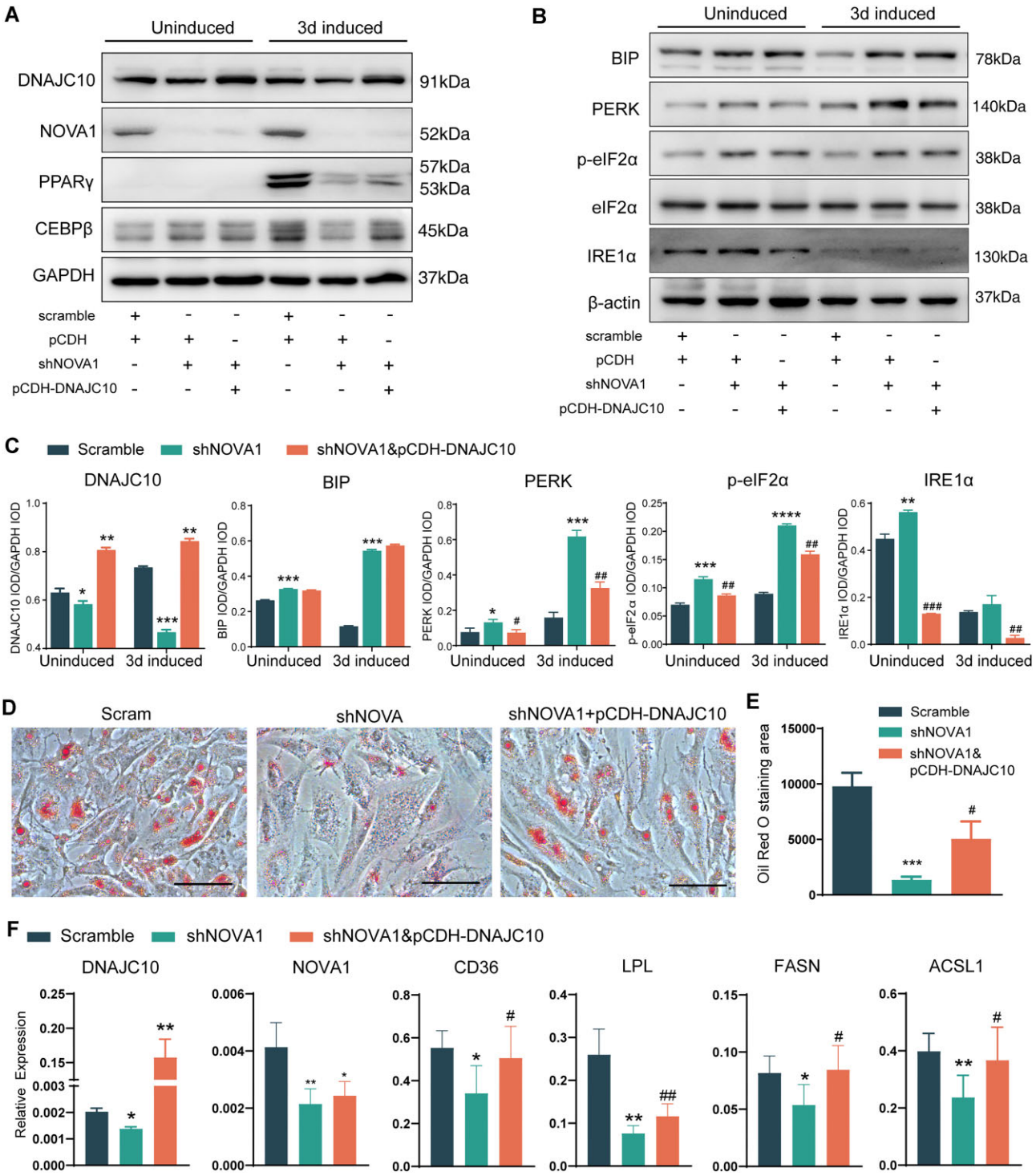

Figure 5. DNAJC10 overexpression rescues the hyperactivation of ER stress and the inhibition of adipogenesis caused by NOVA1 knockdown. (**A**) Western blots for the efficient overexpression of DNAJC10, knockdown of NOVA1 and partially rescued expression of PPARγ and C/EBPβ by DNAJC10 overexpression in NOVA1-deficient hASCs. Blots are representative of three experiments. (**B** and **C**) Western blots and IOD (integrated optical density) quantification data for DNAJC10 overexpression ameliorating the hyperactivation of PERK, p-eIF2α and IRE1α in NOVA1-knockdown hASCs under both undifferentiated and adipogenically induced conditions ($n = 3$). (**D** and **E**) Oil Red O staining and quantification of 7 day adipogenically induced hASCs transduced with control, shNOVA1 and shNOVA1 plus DNAJC10-overexpressing lentivirus, respectively ($n = 3$, scale bar = 100 μm). (**F**) Rescued expression of adipogenic markers by DNAJC10 overexpression in NOVA1-knockdown hASCs after adipogenic induction for 7 days. (*, versus scram with the same adipogenic status, $n = 3$–4). Data are shown as means ± SEMs. *P*-values indicate Student's two-tailed *t*-test; $*P < 0.05$, $**P < 0.01$, $***P < 0.001$; $\#P < 0.05$, $\#\#P < 0.01$, $\#\#\#P < 0.001$.

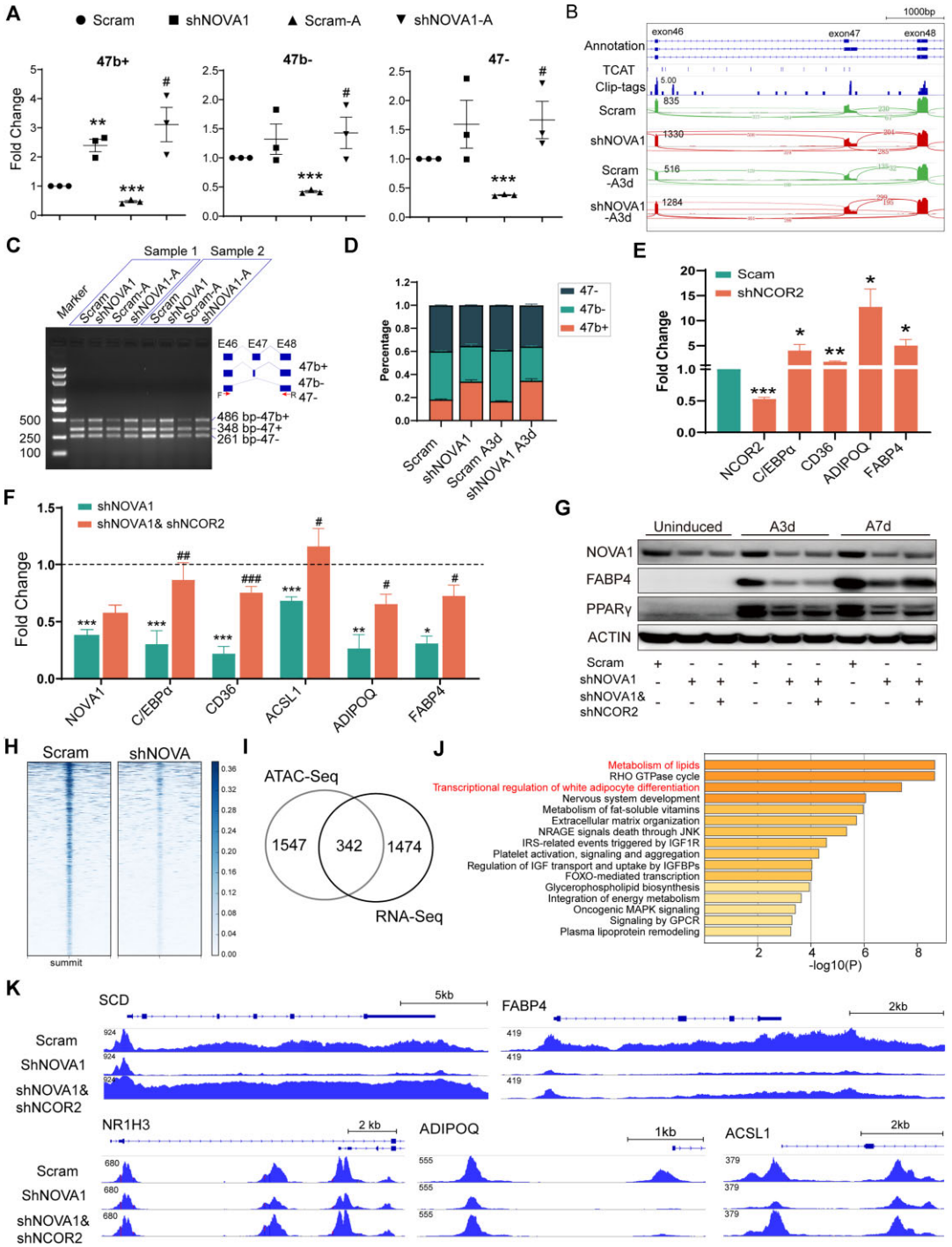

Figure 6. Interruption of the NOVA1–NCOR2 interaction leads to a decrease in chromatin accessibility. (**A**) qPCR analysis showing the dynamic expression of different isoforms of NCOR2 (specific primers span an exon junction of different isoforms) in hASCs with or without NOVA1 knockdown during adipogenesis (*, versus Scram; #, versus Scram-A; $n = 3$). (**B**) IGV representation of CLIP-seq and RNA-seq data at exons 46–48 of the NCOR2 locus. The *y*-axis represents coverage values. Numbers on the plots indicate the values of splice junction reads. Images are representative of two experiments. (**C**) RT-PCR results showing the changed splicing pattern of NCOR2 at exon 47 in control or NOVA1-deficient hASCs before and after adipogenic induction. The scheme on the right illustrates the alternative splicing of NCOR2 at exon 47. The A5SS of exon 47 generates both the longer (47b+) and the shorter isoform (47b–), whereas the exclusion of exon 47 generates the 47– isoform. Primers are indicated by red arrows. Gels are representative of four experiments. (**D**) Quantitative analysis of the percentage of 47b+, 47b– and 47– isoforms. (**E**) Expression of adipogenic marker genes in NCOR2 knockdown hASCs after adipogenic differentiation (*, versus Scram, $n = 4$). (**F** and **G**) Expression and western blots for adipogenic marker genes rescued by NCOR2 knockdown in NOVA1-deficient hASCs during adipogenesis (*, versus Scram; #, versus shNOVA1; $n = 3$). (**H**) Down-regulated ATAC-seq signals from –3 kb to +3 kb surrounding the center of each peak after NOVA1 knockdown. (**I**) Integration of ATAC-seq and RNA-seq data displaying 342 genes with decreased chromatin accessibility and reduced mRNA expression. (**J**) The above 342 genes are enriched in adipogenesis and lipid metabolism. (**K**) IGV representation of ATAC-seq at the loci of lipid metabolism-related genes such as *SCD*, *FABP4*, *NR1H3* (*LPCAT3*), *ADIPQ* and *ACSL1*. Data are shown as means ± SEMs. *P*-values indicate Student's two-tailed *t*-test; $*P < 0.05$, $**P < 0.01$, $***P < 0.001$; $\#P < 0.05$, $\#\#P < 0.01$, $\#\#\#P < 0.001$.

expression of NCOR2 and promotes the exclusion of exon 47b.

Moreover, we also noted that all three isoforms of NCOR2 were down-regulated during adipogenesis (Scram-A versus Scram, Figure 6A), which is consistent with its role as a repressor of nuclear receptors (28). To verify the effect of NOVA1–NCOR2 interaction on adipogenesis, the expression of NCOR2 was knocked down using a specific shRNA targeting exon 47b+. Although the 47b+ isoforms were preferentially knocked down, we observed that the 47b– and 47– isoforms were also down-regulated (Supplementary Figure S4E), probably due to the binding of shRNA with pre-mRNA of NCOR2. NCOR2 knockdown resulted in increased expression levels of adipogenic signature genes in hASCs and rescued the NOVA1 deficiency-induced impairment of adipogenesis (Figure 6E–G). Thus, the results indicate that NOVA1-regulated expression and splicing of NCOR2 participate in the adipogenesis of hASCs.

In addition, as NCOR2 recruits HDACs to regulate chromatin structure and gene expression (30), we applied ATAC-seq to observe the influence of the NOVA1–NCOR2 interaction on chromatin accessibility and its effects on the differentiation potential of hASCs. To do this, hASCs from two biological replicates were pre-infected with lentiviruses encoding scramble, shNOVA1, and shNOVA1 and shNCOR2, respectively, and adipogenically induced for 3 days. We aligned reads genome-wide and defined all open chromatin regions (peaks) in all three groups of cells. The data showed comparable peak fold enrichment distribution across samples and open chromatin distribution along the genome, with expected enrichment at promoters (Supplementary Figure S5A–E). To specifically assess the chromatin-remodeling effects of NOVA1 in preadipocytes, we compared NOVA1-knockdown cells with the scramble controls, and defined 15 128 down-regulated peaks, corresponding to 1889 protein-coding genes, which showed a remarkable association with nervous system development, lipid metabolism and extracellular matrix processes (Supplementary Figure S5F). Integration of ATAC-seq and RNA-seq data revealed 342 genes with decreased chromatin accessibility and reduced mRNA expression, which were enriched in the processes involved in adipogenesis and lipid metabolism (Figure 6I, J). Then we focused on defining whether NOCR2 up-regulation played a role in NOVA1 deficiency-induced chromatin remodeling by comparing differences between the shNCOR2 + shNOVA1 group and shNOVA1 cells. This analysis defined a set of 1872 up-regulated peaks specifically enriched after NCOR2 knockdown, corresponding to 783 protein-coding genes remarkably associated with the extracellular matrix and lipid metabolism (Supplementary Figure S5G, H). Visualization of ATAC-seq revealed that NOVA1 knockdown led to decreased chromatin accessibility at the loci of lipid metabolism-related genes, such as *SCD*, *FABP4*, *NR1H3* (*LPCAT3*), *ADIPQ*, *ACSL1*, *FASN*, *CD36*, *LPL* and *ACACB* (Figure 6K; Supplementary Figure S5I). It is worth noting that NCOR2 knockdown rescued the decrease in chromatin accessibility at the above gene loci in NOVA1-deficient hASCs, with patterns similar to those of the transcriptomic profiles.

NOVA1-regulated white adipogenesis is species specific

Next, we established Nova1$^{flox/flox}$ mice to study the *in vivo* roles of NOVA1 in ASC adipogenesis by crossing to Pdgfra-Cre ERT mice (Figure 7A; Supplementary Figure S5A–D). As subcutaneous adipocyte commitment and differentiation are initiated during days E14–E18 (31), we delivered tamoxifen to E15.5 pregnant mice to induce Cre recombination (Figure 7A). When cesarean sections were performed at day E18.5, no significant abnormalities in development or body size among the pups were observed. While the weights of both Pdgfra-CreER$^{-/-}$;Nova1$^{f/f}$ (Cre–, serve as a control) and Pdgfra-CreER$^{+/-}$;Nova1$^{f/f}$ (Nova1-iKO) mice increased with growth, no significant difference was observed between them (Figure 7B). MRI at the age of 4 months showed that female and male Nova1-iKO mice had similar volumes and distributions of various adipose depots to that of controls, such as inguinal, gonadal and retroperitoneal fat, which was further visualized by the 3D construction of adipose tissue of Nova1-iKO mice (Figure 7C). The volume ratio of adipose tissue to the whole body and that of intraperitoneal adipose tissue (iAT) to subcutaneous adipose tissue (sAT) did not significantly differ between the control and Nova1-deficient mice of either sex (Figure 7D). Hematoxylin & Eosin (H&E) staining of inguinal and gonadal adipose tissue also showed similar adipocyte size and constitution between the control and Nova1-iKO mice (Figure 7E). These results suggest that Nova1 possesses a minimal effect on white adipose tissue development in mice.

We further checked the expression of NOVA1 during adipogenic differentiation of ASCs isolated from the inguinal adipose depot of wild-type mice (mASCs). While adipogenic markers such as *Adipoq*, *Cd36* and *Fabp4* increased, the expression of both Nova1 and Nova2 remained unchanged (Figure 7F). This was confirmed by reanalyzing the adipogenesis transcriptome data of different mouse cell lines including 3T3-L1 cells, C3H10T1/2 and WAT preadipocytes (32–34) (Figure 7G). Moreover, in contrast to the hASCs, RNA-seq analysis of mASCs from both Nova1-iKO and control mice revealed that adipogenesis and UPR gene sets were not violated by NOVA1 deficiency, showing the same increasing or decreasing tendency in Nova1-deficient cells as that in controls during the adipogenic process (Figure 7H). These results indicate that the adipogenic differentiation potential of mASCs is hardly disturbed by NOVA1 deficiency, suggesting that NOVA1 has different effects on white adipogenesis in humans and mice.

To explain the non-significant effects of Nova1 on adipogenesis in mice, we compared the splicing patterns and expression levels of Dnajc10 and Ncor2 in wild-type and Nova1-deficient mASCs. RNA-seq results showed that A3SS splicing at exon 11 (a homolog to human exon 12) did not exist in mice at all (Supplementary Figure S6E). Interestingly, searching the UCSC genome database, we found that the A3SS splicing of DNAJC10 exon 12, which leads to NMD of DNAJC10 due to the partial inclusion of intron 11 and a premature stop codon, only exists in humans (Supplementary Figure S6F). Therefore, we compared the length of the alternatively spliced exon and upstream intron of multiple species and found that the alternatively spliced exons of different species are all 90 bp, whereas the introns

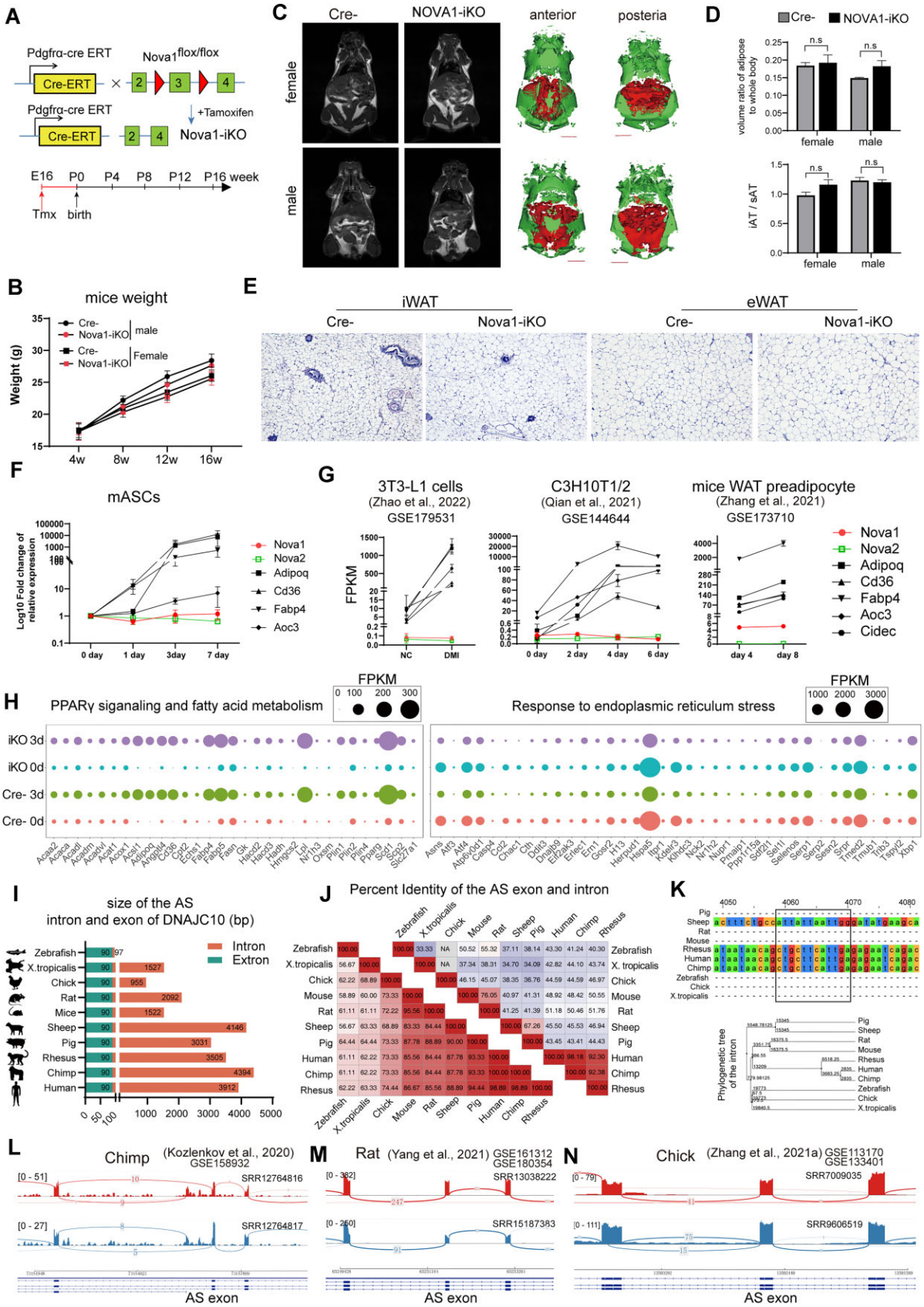

Figure 7. Nova1 is not required for white adipogenesis in mice. (**A**) Schematic diagram explaining the generation of tamoxifen-induced Nova1 exon 3 conditional knockout mice in Pdgfra^{+} adipose stroma cells (Nova1-iKO) and the overall experimental design. (**B**) Comparison of the time-series weight

are variable from ∼4000 bp in primates to 97 bp in zebrafish (Figure 7I). Multiple sequence alignment also showed that the sequences of the alternatively spliced exon are highly similar among species; the percentage identity was 85.56% between humans and mice and even reached 61.11% between humans and zebrafish (Figure 7J). However, the alternatively spliced intron sequences were much less similar among species, except for that among primates (>92%), between mice and rats, and between pigs and sheep. Akin to the sequence identity heatmap, the phylogenetic analysis based on the alternatively spliced intron exhibited evolutionary clustering of animals (Figure 7K, upper). Furthermore, multiple sequence alignment of the alternatively spliced introns showed that the splicing site and pre-stop codon observed in humans could only be found in primates, not in mice, rats and other species (Figure 7K, lower). To confirm this, we reanalyzed the publicly deposited multispecies RNA-seq datasets of adipose and neural tissues or cells where a high level of Nova1 is expressed (35–37). The A3SS event at the alternatively spliced intron of DNAJC10 was observed in chimps, but not in rats and chicks (Figure 7L–N). Similar to that in humans, mice Ncor2 was also spliced into three isoforms at the splicing site of exon 47. However, in contrast to hASCs, the splicing patterns were not changed, and the down-regulated expression of all Ncor2 isoforms during adipogenesis was not disturbed in Nova1 knockout cells (Supplementary Figure S6G–I). The splicing of NCOR2 exon 47 has been identified as a divergent evolutionary event; the existence and proportion of each splicing variant are distinct in species (38). We compared the upstream and downstream introns of exon 47 and found that both introns are larger in humans than in mice (Supplementary Figure S6J). These results are consistent with the active roles of the intron in gene evolution and suggest that the AS of DNAJC10 and NCOR2 may be evolutionarily regulated.

DISCUSSION

Due to the critical roles of adipose tissue in metabolic homeostasis, a better understanding of adipogenesis beyond transcriptional networks would facilitate the development of novel strategies to improve human metabolic diseases. In the current study, we found a regulatory map of the RBP NOVA1 during human white adipogenesis and proved that it coordinates ER and chromatin function by regulating the expression and splicing of DNAJC10 and NCOR2. Surprisingly, NOVA1 was not required and the AS of Ncor2 and Dnajc10 was not regulated by NOVA1 during white adipogenesis of mice. Our findings provide evidence for human-specific roles of NOVA1 in adipogenesis and extend insights into the functionality of RBPs.

The ER is central to protein synthesis, post-translational modification, folding and trafficking, as well as calcium homeostasis and lipid synthesis (39). ER homeostasis may be disturbed by various physiological or pathological stimuli, resulting in the accumulation of misfolded proteins, excessive or damaged lipids and calcium imbalance, which is referred to as ER stress. UPR signaling pathways including PERK–eIF2α, IRE1α/XBP1 and ATF6α are subsequently activated (40). The UPR is tightly intertwined with lipid metabolism. The loss of UPR function by deletions of UPR signals such as PERK, ATF4 and XBP-1 or defective eIF2α phosphorylation greatly attenuates lipogenesis *in vitro* and reduces fat pad mass *in vivo* (41–44), suggesting that the UPR is indispensable for adipogenesis. Moreover, constitutive activation of PERK or an exogenous ER stress stimulator also significantly reduced lipid accumulation and the expression of mature adipocyte markers (45,46). In our study, we found that the UPR was slightly activated during the early adipogenic differentiation of hASCs, whereas thapsigargin or tunicamycin treatment significantly impaired the process, indicating that physiological UPR activation facilitates adipogenesis and severe UPR activation would otherwise have an inhibitory effect on the process. More importantly, we found that NOVA1 knockdown induced a severe UPR in hASCs, while its overexpression acted against the ER stress-stimulating effects of thapsigargin and tunicamycin. These findings suggest that NOVA1 protects the UPR from hyperactivation, which has significant meaning not only in adipogenesis but also in ER dysfunction-related diseases.

In our study, it is worth noting that aberrant DNAJC10 splicing induced by NOVA1 knockdown led to hyperactivation of the UPR and impairment of adipogenesis. DNAJC10 is an ER co-chaperone and functions as an ER-localized disulfide reductase that enhances ER-associated degradation (ERAD) through its associations with EDEM and the ER stress sensor BIP (27). Human DNAJC10 has been observed with multiple alternatively spliced

←

gain of female and male controls and Nova1-iKO mice ($n = 5$–8) (**C**) T1-weighted MRI images showing the distribution of adipose tissues of the 4-month-old control and Nova1-iKO mice induced at day E15.5. Three-dimensional construction of subcutaneous (sAT, green) and intraperitoneal adipose tissue (iAT, red) of female and male Nova1-iKO mice (scale bar = 10 mm). Images are representative of four experiments. (**D**) Comparison of the percentage of whole-body adipose tissue volume and iAT/sAT ratio between control and Nova1-iKO mice ($n = 3$–4). (**E**) H&E staining images of male inguinal (iWAT) and epididymal adipose tissue (eWAT). Images are representative of five experiments. (**F**) Dynamic expression of Nova1, Nova2 and adipogenic markers during the adipogenesis of mASCs isolated from iWAT ($n = 3$). (**G**) Meta-analysis of the expression of Nova1, Nova2 and adipogenesis marker genes during the adipocyte differentiation of 3T3-L1, C3H10T1/2 and pre-adipocytes. (**H**) Bubble charts showing the expression of genes within the corresponding biological processes in uninduced or 3 day induced ASCs isolated from the iWAT of control and Nova1-iKO mice. The size of the bubble indicates the FPKM value of listed genes revealed by RNA-seq analysis of three biological replicates. (**I**) Cross-species comparison of the lengths of the exon and intron analog with the alternative spliced human exon 12 and intron 11, showing the variations of the length of introns. (**J**) Percentage identity matrix generated by multiple sequence alignment demonstrating the fewer similarities between introns of multiple species than between exons. (**K**) Multispecies sequence alignment of the alternatively spliced intron (upper) and phylogenetic tree based on the alternatively spliced intron (lower). Humans, chimps and rhesus monkeys show identical sequences and an in-frame premature stop codon (boxed) at the alternatively spliced site. (**L**–**N**) IGV visualization of multispecies RNA-seq data showing that the AS event of DNAJC10 found in humans is also observed in chimps, but not in rats or chicks. SRR12764816 and SRR12764817, chimp glutamatergic neurons; SRR13038222, rat subcutaneous adipose-derived mesenchymal stem cells; SRR15187383, rat hippocampal CA1 region; SRR7009035, chicken abdominal fat tissue; SRR9606519, chicken brain tissue. The images are representive of three experiments. Data are shown as means ± SEMs. *P*-values indicate Student's two-tailed *t*-test.

transcripts. We found that NOVA1 deficiency increased the retention of intron 11 of DNAJC10 with an in-frame premature stop codon triggering NMD. The same AS-mediated post-transcriptional regulation of DNAJC10 is also observed in neurons (47). Motor neurons differentiated from induced pluripotent stem cells (iPSCs) of spinal muscular atrophy (SMA) patients express less DNAJC10 protein due to a higher level of intron-retained DNAJC10 than wild-type motor neurons; knockdown of DNAJC10 in motor neurons results in elevated expression of chronic ER stress markers and accelerates motor neuron death. Indeed, loss of DNAJC10 and ER stress overactivation, as well as NOVA, have been independently reported to be linked to neurodegeneration in animal models and humans (48–51). However, the correlation among NOVA1, DNAJC10 and ER stress has not been elucidated, and our finding that NOVA1 regulates ER stress through AS of DNAJC10 in adipogenesis might be instructive in understanding neurodegenerative diseases.

Nuclear receptor co-repressors NCoR1 and NcoR2 (also known as NCoR and SMRT, respectively) are central mediators of transcriptional repression, exerting their effects by binding to different nuclear hormone receptors such as TRs, RARs and RXRs (52). NCOR2 has been reported to regulate adipose metabolism; mice with an NCOR2 mutation in the receptor interaction domain exhibit widespread metabolic defects, and cells with NCoR2 deficiency display de-repression of PPARγ and dramatically increased adipogenic capacity (28). Consistent with its role as a repressor, we found that all three isoforms of NCOR2 were dramatically down-regulated during adipogenic differentiation of hASCs. However, NOVA1 knockdown abrogated the decrease in NCOR2 and significantly increased the ratio and expression level of NCOR2 47b+ isoforms (corresponding to SMRTα in previous studies). Exon 47b+ sequences flank only five amino acids downstream of the CoRNR box, a key motif for binding of nuclear receptor partners. The inclusion of exon 47b alters the affinities for different nuclear receptors (29). Therefore, together with the findings that NCOR2 knockdown rescued the reduction of lipid metabolism genes in NOVA1-deficient hASCs, it is reasonable to propose that NOVA1 fine-tunes the binding specificity and capability of NCOR2 by regulating its expression level and splicing pattern.

It has been reported that NCOR2 facilitates transcriptional repression by serving as a scaffold protein to recruit histone deacetylase complexes and chromatin-remodeling factors (30). Integrating ATAC-seq and RNA-seq results, we demonstrated that NOVA1 deficiency led to chromatin remodeling of hASCs with decreased accessibility at the loci of lipid metabolism genes, which could be rescued by the knockdown of NCOR2. In this way, NOVA1 may be taken as a chromatin-remodeling regulator during adipogenesis of human cells. We also found that NOVA1 knockdown led to increased chromatin accessibility of ER stress genes such as HSPA5, XBP1, HERPUD1, ERN1 and EDEM1, suggesting the active transcription of these genes, which is consistent with the up-regulation of ER stress response genes observed in RNA-seq. However, different from the derepressed chromatin loci of adipose metabolism genes due to NCOR2 knockdown, the active chromatin at loci of ER response genes was not restored to an inactive state, indicating that the effects of NCOR2 on adipogenesis may not be attributable to the ER response, at least at the chromatin level. These results further suggested that, in NOVA1-deficient cells, ER stress activation and reduced chromatin accessibility of adipose metabolism genes convergently resulted in the impaired adipogenesis of hADSCs, which is further proved by the results that either DNAJC10 overexpression or NCOR2 knockdown only partially rescued the adipogenesis of NOVA1-deficient hASCs. NCOR2 encodes extremely large proteins composed of 2500 amino acids (molecular mass of 270 kDa), which makes working with them challenging. The mechanism by which NOVA1–NCOR2 interaction regulates the state of chromatin is worthy of further investigation.

Moreover, the regulation of NOVA1 in white adipogenesis was species specific. Using Pdgfra-CreER$^{-/-}$;Nova1$^{f/f}$ mice, we demonstrated that Nova1 is not required during *in vitro* differentiation of mASCs and *in vivo* white adipose tissue development. Previous studies showed that Nova1 was a repressor of brown adipocyte differentiation in mice, and mice deficient in both NOVA1 and NOVA2 in mature adipocytes (driven by Adipoq-Cre) showed increased adipose tissue thermogenesis after being fed a high-fat diet (12,53). Therefore, we propose that NOVA1 plays different roles in adipose tissue metabolism in humans and mice.

We further found that the binding targets of NOVA1 differ among species. Evolutionarily, vertebrates have widely varying phenotypes resulting from species-specific AS, which can affect key regulators of biological processes (54). All three isoforms of NCOR2 exist in both humans and mice, but the existence and proportion of each splicing variant are distinct in these species (38). Here, we showed that neither its splicing patterns nor the expression of its isoforms were disturbed by NOVA1 during white adipogenesis in mice. For DNAJC10, multispecies genome and transcriptome analysis showed that the splicing site and pre-stop codon within DNAJC10 intron 11 and corresponding alternatively spliced isoforms were only observed in primates, not in mice, rats or other non-primate animals. These results are consistent with the active roles of introns in gene evolution. They indicate that NOVA1-regulated DNAJC10 and NCOR2 expression and splicing appear to be evolutionary events.

In summary, though the general regulatory mechanisms of adipogenesis are consistent between humans and mice, such as the impairment of adipogenic potential by overactivation of the UPR and down-regulation of NCOR2 during adipocyte differentiation, the fine-tuning of ER stress and chromatin adaption mediated by NOVA1–DNAJC10 and NOVA1–NCOR2 interactions are specific in humans and may be evolutionarily regulated.

DATA AVAILABILITY

The sequence and array data have been deposited in the National Genomics Data Center under BioProject accession number: PRJCA011678.

SUPPLEMENTARY DATA

Supplementary Data are available at NAR Online.

ACKNOWLEDGEMENTS

We thank Professsor Tao Cheng (Institute of Hematology & Blood Diseases Hospital, CAMS & PUMC, Tianjin) for providing Pdgfra-cre ER mice, and Professors Depei Liu (Institute of Basic Medical Sciences, CAMS & PUMC, Beijing) and Xiaorong Zhang (Institute of Biophysics, CAS, Beijing) for valuable suggestions on the manuscript writing.

FUNDING

The National Natural Science Foundation of China [81873666]; the Chinese Academy of Medical Sciences (CAMS) Innovation Fund for Medical Sciences [2016-I2M-1-17 and 2021-I2M-1-052); and the Non-profit Central Research Institute Fund of CAMS [2018PT32015].
Conflict of interest statement. None declared.

REFERENCES

1. Morigny,P., Boucher,J., Arner,P. and Langin,D. (2021) Lipid and glucose metabolism in white adipocytes: pathways, dysfunction and therapeutics. *Nat. Rev. Endocrinol.*, **17**, 276–295.
2. Ambele,M.A., Dhanraj,P., Giles,R. and Pepper,M.S. (2020) Adipogenesis: a complex interplay of multiple molecular determinants and pathways. *Int. J. Mol. Sci.*, **21**, 4283.
3. Baralle,F.E. and Giudice,J. (2017) Alternative splicing as a regulator of development and tissue identity. *Nat. Rev. Mol. Cell Biol.*, **18**, 437–451.
4. Siang,D.T.C., Lim,Y.C., Kyaw,A.M.M., Win,K.N., Chia,S.Y., Degirmenci,U., Hu,X., Tan,B.C., Walet,A.C.E., Sun,L. *et al.* (2020) The RNA-binding protein HuR is a negative regulator in adipogenesis. *Nat. Commun.*, **11**, 213.
5. Wu,R., Cao,S., Li,F., Feng,S., Shu,G., Wang,L., Gao,P., Zhu,X., Zhu,C., Wang,S. *et al.* (2022) RNA-binding protein YBX1 promotes brown adipogenesis and thermogenesis via PINK1/PRKN-mediated mitophagy. *FASEB J.*, **36**, e22219.
6. Huot,M.E., Vogel,G., Zabarauskas,A., Ngo,C.T., Coulombe-Huntington,J., Majewski,J. and Richard,S. (2012) The Sam68 STAR RNA-binding protein regulates mTOR alternative splicing during adipogenesis. *Mol. Cell*, **46**, 187–199.
7. Buckanovich,R.J., Yang,Y.Y. and Darnell,R.B. (1996) The onconeural antigen Nova-1 is a neuron-specific RNA-binding protein, the activity of which is inhibited by paraneoplastic antibodies. *J. Neurosci.*, **16**, 1114–1122.
8. Jensen,K.B., Dredge,B.K., Stefani,G., Zhong,R., Buckanovich,R.J., Okano,H.J., Yang,Y.Y. and Darnell,R.B. (2000) Nova-1 regulates neuron-specific alternative splicing and is essential for neuronal viability. *Neuron*, **25**, 359–371.
9. Dredge,B.K. and Darnell,R.B. (2003) Nova regulates GABA(A) receptor gamma2 alternative splicing via a distal downstream UCAU-rich intronic splicing enhancer. *Mol. Cell. Biol.*, **23**, 4687–4700.
10. Yuan,Y., Xie,S., Darnell,J.C., Darnell,A.J., Saito,Y., Phatnani,H., Murphy,E.A., Zhang,C., Maniatis,T. and Darnell,R.B. (2018) Cell type-specific CLIP reveals that NOVA regulates cytoskeleton interactions in motoneurons. *Genome Biol.*, **19**, 117.
11. Villate,O., Turatsinze,J.V., Mascali,L.G., Grieco,F.A., Nogueira,T.C., Cunha,D.A., Nardelli,T.R., Sammeth,M., Salunkhe,V.A., Esguerra,J.L. *et al.* (2014) Nova1 is a master regulator of alternative splicing in pancreatic beta cells. *Nucleic Acids Res.*, **42**, 11818–11830.
12. Vernia,S., Edwards,Y.J., Han,M.S., Cavanagh-Kyros,J., Barrett,T., Kim,J.K. and Davis,R.J. (2016) An alternative splicing program promotes adipose tissue thermogenesis. *Elife*, **5**, e17672.
13. Lin,J.C., Lu,Y.H., Liu,Y.R. and Lin,Y.J. (2016) RBM4a-regulated splicing cascade modulates the differentiation and metabolic activities of brown adipocytes. *Sci. Rep.*, **6**, 20665.
14. Yang,Z., Dong,P., Fu,X., Li,Q., Ma,S., Wu,D., Kang,N., Liu,X., Yan,L. and Xiao,R. (2015) CD49f acts as an inflammation sensor to regulate differentiation, adhesion, and migration of human mesenchymal stem cells. *Stem Cells*, **33**, 2798–2810.
15. Ramirez-Zacarias,J.L., Castro-Munozledo,F. and Kuri-Harcuch,W. (1992) Quantitation of adipose conversion and triglycerides by staining intracytoplasmic lipids with oil red O. *Histochemistry*, **97**, 493–497.
16. Zhou,Y., Zhou,B., Pache,L., Chang,M., Khodabakhshi,A.H., Tanaseichuk,O., Benner,C. and Chanda,S.K. (2019) Metascape provides a biologist-oriented resource for the analysis of systems-level datasets. *Nat. Commun.*, **10**, 1523.
17. Chen,J., Cai,Z., Bai,M., Yu,X., Zhang,C., Cao,C., Hu,X., Wang,L., Su,R., Wang,D. *et al.* (2018) The RNA-binding protein ROD1/PTBP3 cotranscriptionally defines AID-loading sites to mediate antibody class switch in mammalian genomes. *Cell Res.*, **28**, 981–995.
18. Machanick,P. and Bailey,T.L. (2011) MEME-ChIP: motif analysis of large DNA datasets. *Bioinformatics*, **27**, 1696–1697.
19. Shen,L., Shao,N., Liu,X. and Nestler,E. (2014) ngs.Plot: quick mining and visualization of next-generation sequencing data by integrating genomic databases. *BMC Genomics*, **15**, 284.
20. Bajic,M., Maher,K.A. and Deal,R.B. (2018) Identification of open chromatin regions in plant genomes using ATAC-Seq. *Methods Mol. Biol.*, **1675**, 183–201.
21. Waterhouse,A.M., Procter,J.B., Martin,D.M., Clamp,M. and Barton,G.J. (2009) Jalview Version 2—a multiple sequence alignment editor and analysis workbench. *Bioinformatics*, **25**, 1189–1191.
22. Potolitsyna,E., Hazell Pickering,S., Germier,T., Collas,P. and Briand,N. (2022) Long non-coding RNA HOTAIR regulates cytoskeleton remodeling and lipid storage capacity during adipogenesis. *Sci. Rep.*, **12**, 10157.
23. Zhang,J., Xu,E., Ren,C., Yan,W., Zhang,M., Chen,M., Cardiff,R.D., Imai,D.M., Wisner,E. and Chen,X. (2014) Mice deficient in Rbm38, a target of the p53 family, are susceptible to accelerated aging and spontaneous tumors. *Proc. Natl Acad. Sci. USA*, **111**, 18637–18642.
24. Hirota,M., Kitagaki,M., Itagaki,H. and Aiba,S. (2006) Quantitative measurement of spliced XBP1 mRNA as an indicator of endoplasmic reticulum stress. *J. Toxicol. Sci.*, **31**, 149–156.
25. Ule,J., Stefani,G., Mele,A., Ruggiu,M., Wang,X., Taneri,B., Gaasterland,T., Blencowe,B.J. and Darnell,R.B. (2006) An RNA map predicting Nova-dependent splicing regulation. *Nature*, **444**, 580–586.
26. Licatalosi,D.D., Mele,A., Fak,J.J., Ule,J., Kayikci,M., Chi,S.W., Clark,T.A., Schweitzer,A.C., Blume,J.E., Wang,X. *et al.* (2008) HITS-CLIP yields genome-wide insights into brain alternative RNA processing. *Nature*, **456**, 464–469.
27. Maegawa,K.I., Watanabe,S., Noi,K., Okumura,M., Amagai,Y., Inoue,M., Ushioda,R., Nagata,K., Ogura,T. and Inaba,K. (2017) The highly dynamic nature of ERdj5 is key to efficient elimination of aberrant protein oligomers through ER-associated degradation. *Structure*, **25**, 846–857.
28. Nofsinger,R.R., Li,P., Hong,S.H., Jonker,J.W., Barish,G.D., Ying,H., Cheng,S.Y., Leblanc,M., Xu,W., Pei,L. *et al.* (2008) SMRT repression of nuclear receptors controls the adipogenic set point and metabolic homeostasis. *Proc. Natl Acad. Sci. USA*, **105**, 20021–20026.
29. Goodson,M.L., Jonas,B.A. and Privalsky,M.L. (2005) Alternative mRNA splicing of SMRT creates functional diversity by generating corepressor isoforms with different affinities for different nuclear receptors. *J. Biol. Chem.*, **280**, 7493–7503.
30. Li,J., Wang,J., Wang,J., Nawaz,Z., Liu,J.M., Qin,J. and Wong,J. (2000) Both corepressor proteins SMRT and N-CoR exist in large protein complexes containing HDAC3. *EMBO J.*, **19**, 4342–4350.
31. Wang,Q.A., Tao,C., Gupta,R.K. and Scherer,P.E. (2013) Tracking adipogenesis during white adipose tissue development, expansion and regeneration. *Nat. Med.*, **19**, 1338–1344.
32. Zhao,Z., Wang,C., Jia,J., Wang,Z., Li,L., Deng,X., Cai,Z., Yang,L., Wang,D., Ma,S. *et al.* (2022) Regulatory network of metformin on adipogenesis determined by combining high-throughput sequencing and GEO database. *Adipocyte*, **11**, 56–68.
33. Qian,H., Zhao,J., Yang,X., Wu,S., An,Y., Qu,Y., Li,Z., Ge,H., Li,E. and Qi,W. (2021) TET1 promotes rxralpha expression and adipogenesis through DNA demethylation. *Biochim. Biophys. Acta*, **1866**, 158919.
34. Zhang,P., Sheng,M., Du,C., Chao,Z., Xu,H., Cheng,X., Li,C. and Xu,Y. (2021) Assessment of circRNA expression profiles and potential functions in brown adipogenesis. *Front. Genet.*, **12**, 769690.
35. Kozlenkov,A., Vermunt,M.W., Apontes,P., Li,J., Hao,K., Sherwood,C.C., Hof,P.R., Ely,J.J., Wegner,M., Mukamel,E.A. *et al.*

(2020) Evolution of regulatory signatures in primate cortical neurons at cell-type resolution. *Proc. Natl Acad. Sci. USA*, **117**, 28422–28432.
36. Yang,C., Zhang,J., Wu,T., Zhao,K., Wu,X., Shi,J., Sun,W. and Kong,X. (2021) Multi-omics analysis to examine gene expression and metabolites from multisite adipose-derived mesenchymal stem cells. *Front. Genet.*, **12**, 627347.
37. Zhang,M., Li,J., Zhu,Y., Wu,Q., Li,Y., Huang,D., Gan,Z., Zhong,L., Huang,J., Li,H. *et al.* (2021) Effect of vitamin E supplementation on deposition and gene expression profiling of abdominal fat in broiler chickens. *J. Poult. Sci.*, **58**, 40–50.
38. Privalsky,M.L. and Goodson,M.L. (2019) Evolution of NCoR-1 and NCoR-2 corepressor alternative mRNA splicing in placental mammals. *BMC Res. Notes*, **12**, 343.
39. Schwarz,D.S. and Blower,M.D. (2016) The endoplasmic reticulum: structure, function and response to cellular signaling. *Cell. Mol. Life Sci.*, **73**, 79–94.
40. Walter,P. and Ron,D. (2011) The unfolded protein response: from stress pathway to homeostatic regulation. *Science*, **334**, 1081–1086.
41. Bobrovnikova-Marjon,E., Hatzivassiliou,G., Grigoriadou,C., Romero,M., Cavener,D.R., Thompson,C.B. and Diehl,J.A. (2008) PERK-dependent regulation of lipogenesis during mouse mammary gland development and adipocyte differentiation. *Proc. Natl Acad. Sci. USA*, **105**, 16314–16319.
42. Rutkowski,D.T., Wu,J., Back,S.H., Callaghan,M.U., Ferris,S.P., Iqbal,J., Clark,R., Miao,H., Hassler,J.R., Fornek,J. *et al.* (2008) UPR pathways combine to prevent hepatic steatosis caused by ER stress-mediated suppression of transcriptional master regulators. *Dev. Cell*, **15**, 829–840.
43. Yoshizawa,T., Hinoi,E., Jung,D.Y., Kajimura,D., Ferron,M., Seo,J., Graff,J.M., Kim,J.K. and Karsenty,G. (2009) The transcription factor ATF4 regulates glucose metabolism in mice through its expression in osteoblasts. *J. Clin. Invest.*, **119**, 2807–2817.
44. Sha,H., He,Y., Chen,H., Wang,C., Zenno,A., Shi,H., Yang,X., Zhang,X. and Qi,L. (2009) The IRE1alpha–XBP1 pathway of the unfolded protein response is required for adipogenesis. *Cell Metab.*, **9**, 556–564.
45. Han,J., Murthy,R., Wood,B., Song,B., Wang,S., Sun,B., Malhi,H. and Kaufman,R.J. (2013) ER stress signalling through eIF2alpha and CHOP, but not IRE1alpha, attenuates adipogenesis in mice. *Diabetologia*, **56**, 911–924.
46. Maris,M., Overbergh,L., Gysemans,C., Waget,A., Cardozo,A.K., Verdrengh,E., Cunha,J.P., Gotoh,T., Cnop,M., Eizirik,D.L. *et al.* (2012) Deletion of C/EBP homologous protein (Chop) in C57Bl/6 mice dissociates obesity from insulin resistance. *Diabetologia*, **55**, 1167–1178.
47. Ng,S.Y., Soh,B.S., Rodriguez-Muela,N., Hendrickson,D.G., Price,F., Rinn,J.L. and Rubin,L.L. (2015) Genome-wide RNA-seq of human motor neurons implicates selective ER stress activation in spinal muscular atrophy. *Cell Stem Cell*, **17**, 569–584.
48. Hasegawa,T., Yoshida,S., Sugeno,N., Kobayashi,J. and Aoki,M. (2017) DnaJ/Hsp40 family and Parkinson's disease. *Front. Neurosci.*, **11**, 743.
49. Munoz-Lobato,F., Rodriguez-Palero,M.J., Naranjo-Galindo,F.J., Shephard,F., Gaffney,C.J., Szewczyk,N.J., Hamamichi,S., Caldwell,K.A., Caldwell,G.A., Link,C.D. *et al.* (2014) Protective role of DNJ-27/ERdj5 in *Caenorhabditis elegans* models of human neurodegenerative diseases. *Antioxid. Redox Signal.*, **20**, 217–235.
50. Conlon,E.G. and Manley,J.L. (2017) RNA-binding proteins in neurodegeneration: mechanisms in aggregate. *Genes Dev.*, **31**, 1509–1528.
51. De Conti,L., Baralle,M. and Buratti,E. (2017) Neurodegeneration and RNA-binding proteins. *Wiley Interdiscip. Rev. RNA*, **8**, e1394.
52. Mottis,A., Mouchiroud,L. and Auwerx,J. (2013) Emerging roles of the corepressors NCoR1 and SMRT in homeostasis. *Genes Dev.*, **27**, 819–835.
53. Lin,J.C., Chi,Y.L., Peng,H.Y. and Lu,Y.H. (2016) RBM4–Nova1–SRSF6 splicing cascade modulates the development of brown adipocytes. *Biochim. Biophys. Acta*, **1859**, 1368–1379.
54. Gamazon,E.R. and Stranger,B.E. (2014) Genomics of alternative splicing: evolution, development and pathophysiology. *Hum. Genet.*, **133**, 679–687.